AD NUMBER

AD885334

NEW LIMITATION CHANGE

TO

Approved for public release, distribution unlimited

FROM

Distribution authorized to U.S. Gov't. agencies only; Test and Evaluation; 08 JUL 1971. Other requests shall be referred to Army Missile Command, Redstone Arsenal, AL.

AUTHORITY

USMAC ltr 7 Dec 1971

AD885334

Distribution limited to U.S. Gov't. agencies only;
Test and Evaluation; 8 July 71. Other requests
for this document must be referred to Army
Missile Command (AMSMI-RND),
Redstone Arsenal, Ala. 35809.
DD Form 1473, item 10, is not correct.
A Healy
8 July 71

NOTICE

"This research was sponsored by the Advanced Research Projects Agency of the Department of the Defense under ARPA Order 1627 and was monitored by the US Army Missile Command under Contract Number DAAH01-70-C-1106. Views and conclusions expressed herein are the primary responsibility of the author or the contractor and should not be interpreted as representing the official opinion or policy of USAMICOM, ARPA, DOD or any other agency of the Government."

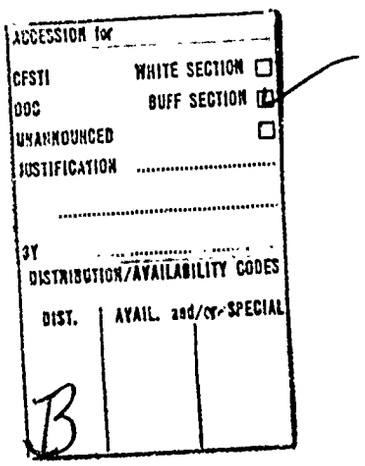

Unclassified

Security Classification

DOCUMENT CONTROL DATA - R&D

(Security classification of title, body of abstract and indexing annotation must be entered when the overall report is classified)

1. ORIGINATING ACTIVITY (Corporate author)	2a. REPORT SECURITY CLASSIFICATION
Hewlett-Packard Company 1501 Page Mill Road Palo Alto, California 94304	Unclassified 2b. GROUP

3. REPORT TITLE

MAGNETIC RARE EARTH COMPOUNDS

4. DESCRIPTIVE NOTES (Type of report and inclusive dates)

Final Technical Report (May 19, 1970 to June 19, 1971)

5. AUTHOR(S) (First name, initial, Last name)

Robert A. Burmeister
Ronald Hiskes
Theron L. Felmlee

6. REPORT DATE	7a. TOTAL NO. OF PAGES	7b. NO. OF REFS
June 1971		37

8a. CONTRACT OR GRANT NO.	9a. ORIGINATOR'S REPORT NUMBER(S)
DAAH01-70-C-1106 b. PROJECT NO. Technical Requirement No. 1335 c. Program Code No. OD10 d. ARPA Order No. 1627	9b. OTHER REPORT NO(S) (Any other numbers that may be assigned this report)

10. DISTRIBUTION STATEMENT This document is subject to special export controls and each transmittal to foreign governments or foreign nationals may be made only with prior approval of the Air Force Avionics Laboratory, Wright-Patterson Air Force Base, Ohio

11. SUPPLEMENTARY NOTES	12. SPONSORING MILITARY ACTIVITY
	Advanced Research Project Agency Department of Defense, Washington, D.C., ARPA Order 1627

13. ABSTRACT

A steady-state crystal growth system suitable for both homoepitaxial and heteroepitaxial growth of unixial magnetic rare earth compounds has been constructed and used for the growth of both $YFeO_3$ and $Eu_2Er_1Ga_{0.7}Fe_{4.3}O_{12}$.

A very stable solvent, comprised of BaO-B_2O_3-BaF_2 has been developed. This solvent is nonvolatile and nonreactive, and is well suited to the solution growth of magnetic oxides.

Arrays of bubbles have been generated in $YFeO_3$ and the coercivity and mobility of crystals grown from this solvent have been measured and found to be ~0.05 Oe and ~3500 cm/s-Oe, comparable to the values for crystals grown in the PbO-based solvents. Stable arrays of mobile bubbles have also been generated in heteroepitaxially grown $Eu_2Er_1Ga_{0.7}Fe_{4.3}O_{12}$.

Emission spectrographic analysis indicates that barium incorporation in the crystals grown from the BaO-based solvent is less than lead incorporated in those grown from the PbO-based solvent.

DD FORM 1 NOV 68 1473 REPLACES DD FORM 1473, 1 JAN 64, WHICH IS OBSOLETE FOR ARMY USE.

Unclassified

Security Classification

14 KEY WORDS	LINK A		LINK B		LINK C	
	ROLE	WT	ROLE	WT	ROLE	WT
Garnets						
Orthoferrites						
Magnetic Bubbles						
Rare Earths						
Crystal Growth						
Epitaxy						
Solution Growth						
$YFeO_3$						
$Eu_2Er_1Ga_{0.7}Fe_{4.2}O_{12}$						
BaO						
Steady-state						

TECHNICAL REQUIREMENT NO. 1335
ARPA Order 1627

MAGNETIC RARE EARTH COMPOUNDS

FINAL TECHNICAL REPORT

June 1971

HEWLETT-PACKARD
COMPANY
Palo Alto, California
94304
(415) 493-1501
Contract No. DAAH01-70-C-1106
Program Code No. OD10

ARPA Support Office
Research, Development, Engineering, and
Missile Systems Laboratory

A Research Project Sponsored by the Advanced
Research Project Agency, Department of
Defense, Washington, D.C., ARPA Order 1627

FOREWORD

This report describes work performed under Contract DAAH01-70-C-1106 for the ARPA Support Office, Research, Development, Engineering, and Missile Systems Laboratory, U.S. Army Missile Command, Redstone Arsenal, Alabama during the period 19 May 1970 through 19 May 1971. The monitors for this project were G. W. Hagood and S. L. Johnston. The work was performed in the Solid-State Laboratory of Hewlett-Packard Laboratories under the direction of P. E. Greene. The work was supervised by R. A. Burmeister, and this report was written by T. L. Felmlee and R. Hiskes.

SUMMARY

A steady-state crystal growth system suitable for both homoepitaxial and heteroepitaxial growth of magnetically uniaxial rare earth compounds was designed, constructed and successfully operated.

A very stable solvent, comprised of $BaO-B_2O_3-BaF_2$ has been developed. This solvent has a low vapor pressure and has been found to be well suited to the solution growth of magnetic compounds, particularly for controlled epitaxial growth at elevated temperatures. Characterization of the solvent indicates the solubility of $YFeO_3$ and the uniaxial rare earth garnets is greater than in the conventional PbO-based solvents.

Both $YFeO_3$ and $Eu_2Er_1Ga_{0.7}Fe_{4.3}O_{12}$ have been grown in this solvent. The $YFeO_3$ has been grown both in bulk form and homoepitaxially on $YFeO_3$ seed crystals. The $Eu_2Er_1Ga_{0.7}Fe_{4.3}O_{12}$ has been grown heteroepitaxially on $Gd_3Ga_5O_{12}$ substrates.

Characterization of magnetic properties has included studies of the generation of straight domain walls and their interaction with crystalline defects, the generation of bubble domains, and the measurement of coercivity and domain wall mobility.

Arrays of bubbles have been generated in $YFeO_3$ grown homoepitaxially in the $BaO-B_2O_3-BaF_2$ solvent, and the coercivity and mobility of crystals grown from this solvent have been measured and found to be ~ 0.05 Oe and

$\sim$3500 cm/s -Oe respectively, comparable to the values obtained elsewhere for crystals grown in the PbO-based solvent. Stable arrays of mobile bubbles have also been generated in $Eu_2Er_1Ga_{0.7}Fe_{4.3}O_{12}$ grown heteroepitaxially by the transient method in PbO-based solvent, but domain wall mobility has not yet been measured in this material.

Emission spectrographic analysis indicated that barium incorporation in the crystals grown from the BaO-based solvent is less than lead incorporated in those grown from the PbO-based solvent, with values ranging from $\sim$150 ppm in $YFeO_3$ grown at $\sim$1300°C to 820 ppm in $YFeO_3$ grown $\sim$1100°C. Values as low as 24 ppm barium have been found for $Eu_2Er_1Ga_{0.7}Fe_{4.3}O_{12}$ grown at 900-1000°C.

TABLE OF CONTENTS

Section		Page
1.0.	INTRODUCTION	1
2.0.	CRYSTAL GROWTH	12
2.1.	General Considerations	12
2.1.1.	The Steady-State Solution Technique	12
2.1.2.	Epitaxial Steady-State Solution Growth	13
2.1.3.	Substrate Selection	15
2.1.4.	Solvent Considerations	17
2.1.4.1.	Interface Stability Analysis	20
2.1.4.2.	Fluid Motion Effects During Solution Crystal Growth	22
2.2.	Experimental Procedures	26
2.2.1.	Apparatus	26
2.2.2.	Preparation of Seeds and Substrates	26
2.2.2.1.	Growth of $YFeO_3$ Seed Crystals for Steady State Bulk Growth	26
2.2.2.2.	Substrate Preparation and Evaluation	28
2.2.3.	Characterization of the $BaO-B_2O_3-BaF_2$ Solvent	32
2.2.3.1.	Liquidus Surface and Solubility of $YFeO_3$ and Rare Earth Garnets	32
2.2.3.2.	Densities of the Crystal Growth Solutions	35
2.2.4.	Steady-State Crystal Growth	40
2.2.4.1.	Orthoferrites	40
2.2.4.1.1.	Procedure	40

TABLE OF CONTENTS
(Continued)

Section		Page
2.2.4.1.2.	Results and Discussion of Bulk Steady-State Growth	43
2.2.4.1.3.	Results and Discussion of Heteroepitaxial Steady-State $YFeO_3$ Growth	48
2.2.4.2.	Heteroepitaxial Growth of Rare Earth Garnet Bubble Compounds	51
3.0.	CHARACTERIZATION AND EVALUATION	60
3.1.	Chemical Analyses	60
3.2.	Lattice Parameter Determination	62
3.3.	Straight Magnetic Domain Wall Apparatus	64
3.4.	Generation and Observation of Bubbles	66
3.4.1.	Coercivity Measurements	66
3.4.2.	Mobility Measurements	69
3.5.	X-ray Topographic Studies	70
4.0.	CONCLUSIONS	72

LIST OF FIGURES

Number		Page
Figure 1.	Comparative Bit Rates for Bubbles in Garnet and Orthoferrite Devices.	7
Figure 2.	Steady-State Liquid Phase Epitaxial Growth Apparatus.	14
Figure 3.	Lattice Parameter Match at $\approx$ 250°C for Iron Garnets and Gallium Garnet Solid Solutions.	16
Figure 4.	$BaO-B_2O_3$ Phase Diagram Depicting Solution Growth Stability Regions for Various Magnetic Materials.	19
Figure 5.	Convective Stability Regime for $BaO-B_2O_3-BaF_2$ Solvent in a Vertical Temperature Gradient.	25
Figure 6.	Schematic of Steady-State Crystal Growth System.	27
Figure 7.	$Gd_3Ga_5O_{12}$ Substrate Material (Sliced and Polished) Millimeter Grid.	29
Figure 8a.	Dislocation Etch Pit Patterns in Syton Polished $\{111\}Gd_3Ga_5O_{12}$ which has been etched in 160°C H_3PO_4 for 20 minutes (100X).	31
Figure 8b.	Growth Striations in a Different Syton Polished $\{111\}$ $Gd_3Ga_5O_{12}$ Substrate which has been Etched in 160°C H_3PO_4 for 20 Minutes. (200X)	31
Figure 9.	Possible Partial Liquidus Projection for $BaO-B_2O_3-BaF_2$ System with a Ternary Eutectic at A.	33
Figure 10.	Solubility Curve for $YFeO_3$ in 21 (Mole)% BaO, 41% B_2O_3, 18% BaF_2.	34
Figure 11.	Tentative Solubility Curve for $Eu_2Er_1Ga_{0.7}Fe_{4.3}O_{12}$ in the BaO-based Solvent.	36

LIST OF FIGURES
(Cont'd)

Figure 12. Temperature Dependence of the Density of Various Crystal Growth Solutions: Solvent Composition 41 (mole)% BaO, 41% B_2O_3 18% BaF_2. 38

Figure 13. Concentration Dependence of the Density for $Eu_2Er_1Ga_{0.7}Fe_{4.3}O_{12}$ in the BaO-Based Solvent. (Temperature = 1050°C) 39

Figure 14. A Slice of $YFeO_3$ Processed from a Crystal Grown in the Steady-State System from a BaO-based Solvent. It is Shown here Containing a Serpentine Magnetic Domain Pattern. (31X) 45

Figure 15. Platelet of $YFeO_3$ Showing Banded Pattern. The Irregularly Shaped Holes Stem from Dissolving Solvent out of Inclusions. (31X) 46

Figure 16. Results of Attempted Heteroepitaxial Growth $YFeO_3$ on an $YAlO_3$ Substrate. Left Portion is $YFeO_3$; Right Portion is Substrate Surface which has been Attacked by Growth Solution. (100X) 50

Figure 17a. {111} $Gd_3Ga_5O_{12}$ Substrate after Attack by PbO-B_2O_3 Solvent in only Slightly Supersaturated Solution at 900°C (19,000X) 53

Figure 17b. Surface Morphology of $Eu_2Er_1Ga_{0.7}Fe_{4.3}O_{12}$ Epitaxial Layer which Grew upon This Rough Surface. (19,000X) 53

Figure 18. Top View of Epitaxial Layer of $Eu_2Er_1Ga_{0.7}Fe_{4.3}O_{12}$ on {111} $Gd_3Ga_5O_{12}$ Substrate Showing Small Scratches in Substrate Enlarging in the Epitaxial Layer. (200X) 55

Figure 19. Crack Pattern in $Eu_2Er_1Ga_{0.7}Fe_{4.3}O_{12}$ Epitaxial Layer Grown on {111} $Gd_3Ga_5O_{12}$ Substrate in BaO-based Solvent. 56

LIST OF FIGURES
(Cont'd)

Figure 20a. Cross Section of $Eu_2Er_1Ga_{0.7}Fe_{4.3}O_{12}$ Epitaxial Layer on {111} $Gd_3Ga_5O_{12}$ Substrate Showing Dendritic Breakdown after ~1 Micron of Growth. (6000 X) (Apparent Roughness in Substrate is a Cleavage Artifact). 58

Figure 20b. $Eu_2Er_1Ga_{0.7}Fe_{4.3}O_{12}$ Epitaxial Layer Top Surface, Showing Breakdown of the Layer to Equilibrium Form Polycrystals (1000X) 58

Figure 20c. Cross Section of $Eu_2Er_1Ga_{0.7}Fe_{4.3}O_{12}$ Epitaxial Layer on {111} $Gd_3Ga_5O_{12}$ Showing Uniform Growth and a Smooth Surface. (2400X) 58

Figure 21. Transition Between Rough and Smooth Regions of $Eu_2Er_1Ga_{0.7}Fe_{4.3}O_{12}$ Epitaxial Layer. (4900X) 59

Figure 22a. Magnetic Domains in Polished Slice of $YFeO_3$ with Small Applied Magnetic Field.(50X) 65

Figure 22b. Magnetic Field Increased Slightly. (50X) 65

Figure 22c. Magnetic Field Increased Enough to Force a Straight Wall Between Two Domains in the $YFeO_3$, Except for "Hang Up" on Defect. (50X) 65

Figure 22d. Same Magnetic Field but Domain Wall Has Been Moved to a Defect-Free Portion of the Crystal. (50X) 65

Figure 23a. Strip Domain in $YFeO_3$ Platelet. (32X) 67

Figure 23b. Bubble Domain Generated from the Strip Domain by Increasing the Bias Field. (32X) 67

Figure 24a. Strip Domains in $Eu_2Er_1Ga_{0.7}Fe_{4.3}O_{12}$. (400X) 68

Figure 24b. Bubble Domains Generated from the Strip Domains by Increasing the Bias Field. (400X) 68

Figure 25a. Optical Transmission Photograph of $YFeO_3$ Platelet Showing Gradually Increasing Optical Absorption Toward the Top of The Platlet. 71

Figure 25a. Lang Topograph of Same Area as Figure 25a, Depicting Optically Invisible Dislocations (Dark Lines and Spots). 71

LIST OF TABLES

Table		Page
Table I.	Properties of Rare Earth Orthoferrites	3
Table II.	Bubble Garnet Compositions and Properties	5
Table III.	Properties of Rare Earth Garnets	6
Table IV.	Parameters for Seeded, Steady-State Growth Runs of $YFeO_3$	41
Table V.	Growth Parameters for Heteroepitaxial $YFeO_3$ Runs in the Steady-State System	42
Table VI.	Typical Impurity Levels Found in $YFeO_3$ Samples Grown from PbO- and BaO-Based Solvents.	61
Table VII.	Cell Dimensions of $YFeO_3$ at Room Temperature (Å)	63

1.0. INTRODUCTION

Magnetic "bubble" domains are localized highly stable cylindrical regions which can exist in certain classes of magnetic materials, notably rare earth orthoferrites and garnets. They can be easily moved about under an applied magnetic field gradient, in much the same way as a charged particle, and thus have generated a great deal of technological interest, particularly because of the promise they hold for efficient, high density (10^7 bits/in^3) information storage. Within the past two years a number of laboratories in this country and abroad have mounted intensive research efforts in the search for new bubble materials and improved methods for synthesizing and characterizing these materials. This effort has in some cases resulted in significant advances as will be described in subsequent sections.

Although prototypes of some practical devices have been constructed, the bright promise of the bubble domain is tempered by the demanding materials requirements for such devices. Some of the stringent requirements for usable material include:

1. thin single crystal plates having uniaxial magnetic anisotropy with the easy axis of magnetization perpendicular to the surface of the plate;
2. very low density of structural imperfections over large areas of the plates (size dictated by specific application).
3. domains generated in such materials must be small enough to allow high storage densities, yet large enough to be

detectable (1μ < diameter < 75μ), and they must be mobile.

4. the magnetic properties of the material must be relatively temperature insensitive at ambient temperature.

The evolution of materials perfection criteria and choice of bubble materials themselves has been extremely rapid, resulting in very significant scientific and technological advances, since Bobeck's original paper in 1967.[1]

The first class of materials to be investigated was the rare earth orthoferrites. $YFeO_3$ is perhaps the most important member of this class. Relevant properties of the orthoferrites are shown in Table I, which indicates stable bubble diameters of 0.75-7.5 mils requiring layer thickness of the same order of magnitude. The orthoferrites also have quite high bubble mobilities, ranging up to 9000 cm/s-Oe for $YFeO_3$[2]. The large bubble diameters place a very stringent requirement upon crystal perfection since 10^4 stable bubbles requires almost one square inch of defect-free material. The congruently melting orthoferrites can be grown by a number of standard techniques, including Bridgman[3] and float zone[4] methods. The boules can then be sliced and polished to 0.75-7.5 mil thickness, and the material is ready for use; however, practical limitations in producing defect-free material of this size have stimulated investigations into other growth techniques.

The most exciting development in the evolution of bubble materials has been the discovery at Bell Laboratories of magnetic bubble domain configurations in the mixed rare earth garnets.[5] These magnetically

TABLE I
Properties of Rare Earth Orthoferrites (2, 16)

Rare Earth	Néel Temperature (°K)	Average Stable Bubble Dia. (mils)	Domain Wall Mobility (cm/sec-Oe)	$4\pi M_s$ (Oe)
Y	646	3.0	9000	105
La				83
Pr				71
Nd	690	7.5		62
Sm	674	6.0		84
Eu	664	5,5	325	83
Gd	663	3.7		94
Tb	651	1.7		137
Dy	643	2.0		128
Ho	643	4.5	200	91
Er	641	6.0	300	81
Tm	631	2.3	750	140
Yb	632	3.8		143
Lu	623			119
$Sm_{0.6}Er_{0.4}$	~660	1.0		83
$Sm_{0.55}Tb_{0.45}$	~670	0.75		108

uniaxial garnets are a compromise between orthoferrites, which have high-domain wall mobility, but large stable bubble diameter, and the hexagonal ferrites, such as magnetoplumbite ($PbFe_{12}O_{19}$) in which the bubble size can be made as small as desired down to 0.2μ, but which have disappointingly low mobilities.[6] Garnets can be tailor-made to obtain desired magnetic characteristics by introducing controlled amounts of up to six different ions in the dodecahedral (rare earth) sites as well as the tetrahedral and octahedral (Fe^{3+}) sites. One class of suitable garnets is obtained when the magnetic moment is optimized ($4\pi M_S \sim 150$ gauss), magnetostriction is made very small and the temperature coefficient of magnetization is small. All the rare earth ions are similar in size and can be easily introduced into the crystal in controlled amounts by appropriately adjusting the melt composition. Examples of some of the bubble garnets prepared to date and the properties of rare earth garnets are given in Tables II and III.

A comparison between the properties of orthoferrites and garnets is shown in Figure 1, which demonstrates bit rate* (cycles/s) versus bubble diameter for several values of mobility. It can be seen that, although the bubble diameters of the orthoferrites are larger than the garnets, the mobility is also higher, making the two classes of compounds comparable in device speed. The width of the shaded regions is fixed by intrinsic properties of the crystals, but vertical expansion may occur (shown by dotted lines) as better quality crystals are produced, resulting in increased bubble mobility.

*This bit rate is the speed with which bubbles may be moved from one T-bar to the next in the drive circuit and is based on a number of (conservative) assumptions. The cycle rate may be expected to increase with the use of more advanced drive circuits.

TABLE II

Bubble Garnet Compositions and Properties *

Garnet Compositions	Growth Technique	Optimum Bubble Diameter (microns)	Mobility (cm/s--Oe)
$Eu_{0.09}Gd_{2.32}Tb_{0.59}Fe_5O_{12}$	Slow-cooled solution growth (bulk)	-	-
$Er_2TbAl_{1.1}Fe_{3.9}O_{12}$	"	7.0	55
$Er_2TbAlFe_4O_{12}$	"	-	-
$Gd_{2.34}Tb_{0.66}Fe_5O_{12}$	"	7.5	120
$Y_{2.25}Tb_{0.75}Ga_{0.9}Fe_{4.1}O_{12}$	"	-	-
$Gd_{0.95}Tb_{0.75}Er_{1.30}Al_{0.5}Fe_{4.5}O_{12}$	"	3.0	60
$Gd_{2.31}Tb_{0.60}Eu_{0.09}Fe_5O_{12}$	"	-	-
$Y_2Gd_1Al_{0.8}Fe_{4.2}O_{12}$	"	2.5	180
$Y_{1.8}Eu_{0.2}Gd_{0.5}Al_{0.6}Fe_{4.4}O_{12}$	"	3.0	186
$TbTm_2Ga_{0.6}Fe_{4.4}O_{12}$	"	-	-
$Eu_2Er_1Ga_{0.7}Fe_{4.3}O_{12}$	Bulk growth and liquid phase epitaxial (LPE) growth on {111} & {110} $Gd_3Ga_5O_{12}$ substrates	5.5	165
$Gd_{3-x}Tb_xFe_5O_{12}$	LPE on {111} $Nd_3Ga_5O_{12}$ substrate	-	-
$Y_{3-x}Gd_xFe_5O_{12}$	LPE on {111} $Gd_3Ga_5O_{12}$ substrate	-	-
$Eu_1Er_2Fe_{4.3}Ga_{0.7}O_{12}$	LPE on {110} & {111} $Gd_3Ga_5O_{12}$ substrates	-	-
$Y_3Ga_xFe_{5-x}O_{12}$	Bulk grown then stressed {111} slices	-	
$Y_3Fe_5O_{12}$	Chemical vapor deposition (CVD) on {111} $Gd_3Ga_5O_{12}$ substrate	-	-
$Y_3Fe_{4.4}Ga_{0.6}O_{12}$	"	8	380
$Tb_{2.4}Er_{0.6}Fe_5O_{12}$	CVD on {100} $Sm_3Ga_5O_{12}$ substrate	8	-

*Data Taken from References 5, 14, 38, 12, 11, 39, 40.

TABLE III
Properties of Rare Earth Garnets (5, 14)

Rare Earth $R_3Fe_5O_{12}$	Lattice Constant (Å)	Neel Temp(°K)	Magnetostriction Constants λ_{111} (x 10^6)	λ_{100} (x 10^6)	$4\pi M_S$
Y	12.376	560	-2.4	-1.4	1767
La					
Pr					(~2100)
Nd					(~2100)
Sm	12.52	560	-8.5	21.0	1675
Eu	12.52	570	1.8	21.0	1172
Gd	12.48	564	-3.1	0.0	56
Tb	12.45	568	12.0	-3.3	198
Dy	12.41	563	-5.9	-12.5	376
Ho	12.38	567	-4.0	-3.4	882
Er	12.35	556	-4.9	2.0	1241
Tm	12.33	549	-5.2	1.4	1397
Yb	12.29	548	-4.5	1.4	1555
Lu	12.28	539	-2.4	-1.4	1815
$Eu_{0.09}Gd_{2.32}Tb_{0.59}Fe_{4.2}Ga_{0.8}O_{12}$			0.0167	-0.0190	150
$Y_3Al_5O_{12}$	12.01				
$Gd_3Ga_5O_{12}$	12.380				
$Nd_3Ga_5O_{12}$	12.505				
$Y_3Ga_5O_{12}$	12.23				

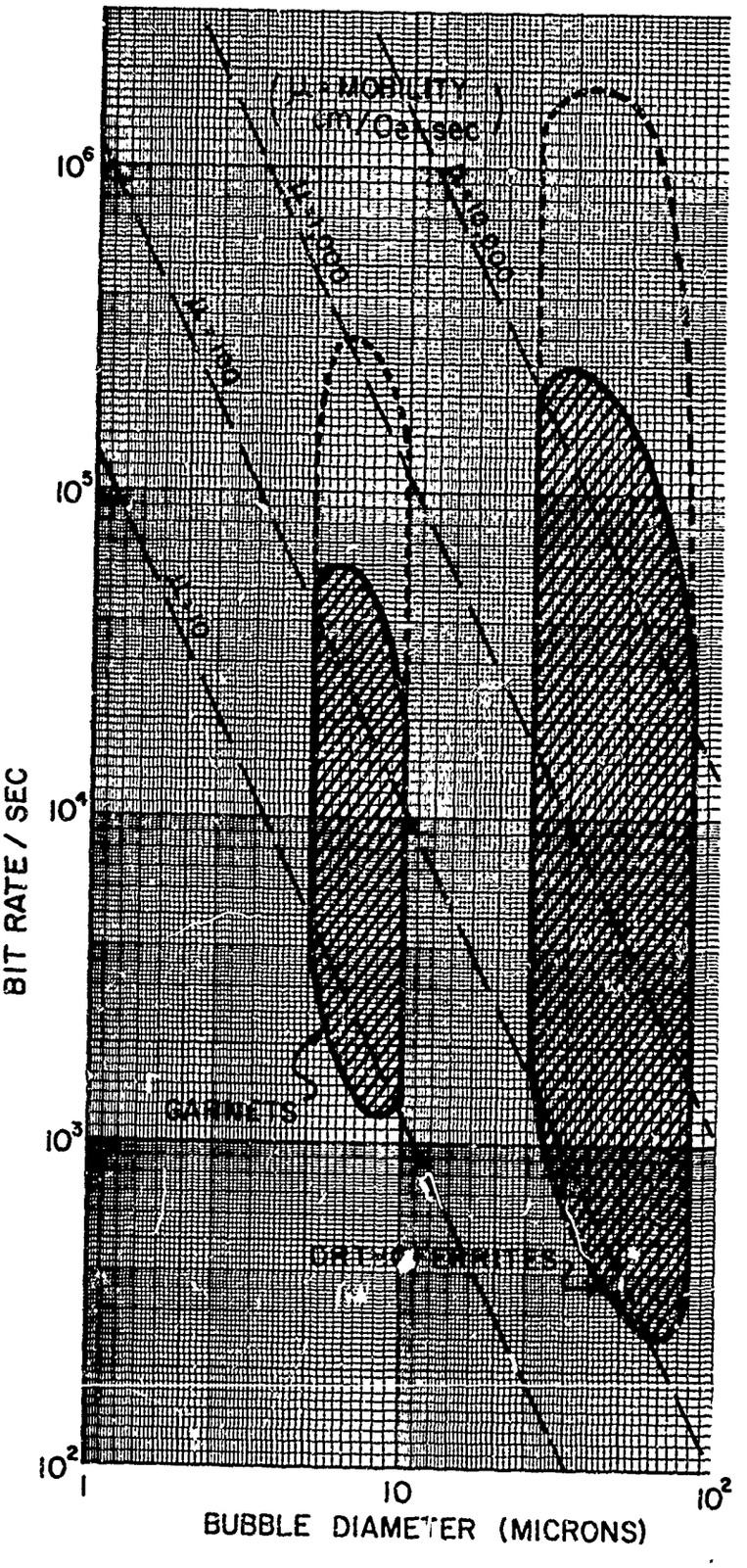

Figure 1. Comparative Bit Rates for Bubbles in Garnet and Orthoferrite Devices.

It is important to note that when these cubic garnets are in thermodynamic equilibrium they should not be magnetically uniaxial. However, there are at present several novel methods of developing the proper uniaxiality depending upon the growth mode utilized. Bulk solution grown garnets (if grown below 1200°C) exhibit a region of uniaxiality beneath certain growth facets. This is attributed in part to a magnetic ordering effect during crystal growth.[7-9] Garnets grown by vapor phase epitaxy are highly strained,[10] and this strain introduces uniaxial anisotropy via magnetostriction. Giess and coworkers[11] have recently investigated this strain induced anisotropy and have induced magnetic bubbles in bulk grown garnets exhibiting no as grown unixiality. They prepared a polished plate and then controllably strained it, thereby mechanically introducing the proper uniaxiality via magnetostriction.

One of the most significant developments in garnet growth has been the liquid phase heteroepitaxial technique developed by Shick et al.[12] Here the uniaxiality is attributed to a magnetic ordering effect during crystal growth in addition to a small amount of strain induced by the difference in thermal expansion coefficients between the epitaxial layer and substrate. Advantages of heteroepitaxy for the growth of magnetic bubble materials are manifold, the most important being the elimination of any processing steps between actual growth of the crystal and its utilization in a device. The nonequilibrium state of the anisotropy has both advantages and disadvantages. Annealing at temperatures above 1200°C will destroy the anisotropy, rendering the layer

useless. Carefully controlled annealing procedures, however, can be used to precisely fix the amount of anisotropy which in turn fixes the bubble size,[13] hence the packing density of the device.

In light of the recent advances in exploratory growth and characterization of the rare earth garnets, these materials currently offer the brightest hope for future development, provided necessary growth techniques can also be developed to obtain precise control over the growth process. Indeed, the very existence of the uniaxiality appears to be closely coupled to the growth process.

It is clear from the discussion above that materials problems are the major limitation to the practical utilization of bubble devices. In view of the technological importance of these devices and the key role of magnetic rare earth compounds, this program was undertaken in an effort to advance the state of the art in the science and technology of these materials. The specific objectives of this program include the following:

1. Development of practical techniques for the growth of single crystals of rare earth compounds having properties suitable for studies and utilization of magnetic domain wall phenomena ("bubble" motion).
2. Acquisition of the necessary data to better characterize and quantitatively describe both the crystal growth process and the salient physical and chemical properties of the crystals produced.

3. Determination of the relationships between methods and parameters of the crystal growth process and the relevant physical properties of the crystals thus grown.

To date, techniques have been developed for the growth of high quality orthoferrites and rare earth garnets which are generally applicable to any class of bubble materials. These crystals have been characterized in an effort to understand interrelationships between their magnetic and other physical properties. The groundwork has thus been laid for correlation between growth parameters and the relevant physical properties of the crystals, which will allow optimization of preparative techniques for these crystals.

The choice of materials for the growth and characterization of the magnetic bubble materials has been dictated by current state-of-the-art knowledge of some of the more fundamental properties of these materials. $YFeO_3$ was chosen as the initial material to be studied in this program, since it is similar in many respects to the balance of the rare earth orthoferrites and thus can be considered typical. Furthermore, it is probably the best characterized bubble material currently available.

As the prospects for uniaxial garnet bubble materials brightened, we initiated growth of several of the rare earth garnets, such as $Eu_2Er_1Ga_{0.7}Fe_{4.3}O_{12}$, which exhibits the necessary unixial unisotropy with a stable bubble size of 5-10 microns,[14] allowing a theoretical packing

density of 10^6 bits/in^2. Thus, for many applications, defect-free areas of less than 1 cm^2 of these materials will be sufficient.

In this program, we have investigated primarily the use of the steady-state solution growth technique. This crystal growth method obviates the homogeneity problems found in the transient techniques, (especially in the mixed cation rare earth garnets) and provides a means for reliable control of the parameters which enhance crystal quality and morphology. The recent availability of substrates of suitable quality for the epitaxial growth of the orthoferrites and garnets have allowed us to examine the heteroepitaxial growth of these materials. The generality and applicability of results obtained in this program to a variety of magnetic rare earth compounds will become apparent in the following sections.

2.0. CRYSTAL GROWTH

2.1. Introduction

Crystal growth techniques for device applications are dictated primarily by device requirements and the choice of material. As mentioned previously, the orthoferrites can be grown by a bulk process (either solution or melt growth) and then sliced and polished to convenient size ($\sim$ 50-100 microns thick). However, the rare earth bubble garnets require slices 5-20 microns thick, too thin to conveniently handle if unsupported. They must, therefore, be grown epitaxially on a suitable substrate in order to best exploit their device capabilities.

Some of the mixed garnets being considered for bubble devices contain up to six different metallic cations, which must be distributed in a controlled fashion over large regions of the crystal. The amount of incorporation of each cation depends upon the ratio of its concentration in a saturated liquid in contact with the solid garnet, which in general is different for each cation. Van Uitert[5] noted a marked exponential dependence of the distribution coefficient upon rare earth ion radius, and each of these distribution coefficients may be itself a complex function of temperature, so that it is impossible to avoid composition excursions in the crystal unless the interface temperature is kept constant.

2.1.1 The Steady-State Solution Growth Technique

Steady-state solution growth techniques meet these requirements for both orthoferrites and garnets, and have none of the disadvantages inherent

in many other relevant growth methods.[15] This process has not been investigated in detail by others except as noted in Reference (15). The steady-state solution technique used in this study is, in essence, growth in a thermal gradient. The growth occurs at constant temperature on a seed crystal or substrate held in a cool portion of a solution which is saturated by by a source of crystal constituents in a hot zone of the same solution as shown in Figure 2. Advantages accruing from this approach are:

1. optimum control of nucleation, since large supercooling is avoided by heterogeneous nucleation on a structurally similar seed or substrate;
2. precise interface temperature and interface gradient control to permit optimum growth without interface breakdown;[15]
3. constant interface temperature to enhance proper distribution of cations in the crystal lattice of the mixed rare earth garnets.

The principal limitation of the bulk solution technique is the length of time required to grow crystals of centimeter size or larger, which ranges from two-six weeks.

2.1.2. Epitaxial Steady-State Solution Growth

Liquid phase epitaxy (LPE) is of particular interest for the growth of materials for bubble device applications, as noted earlier. Relevant substrates, such as $YAlO_3$ for the orthoferrites, and nonmagnetic gallium substituted garnets

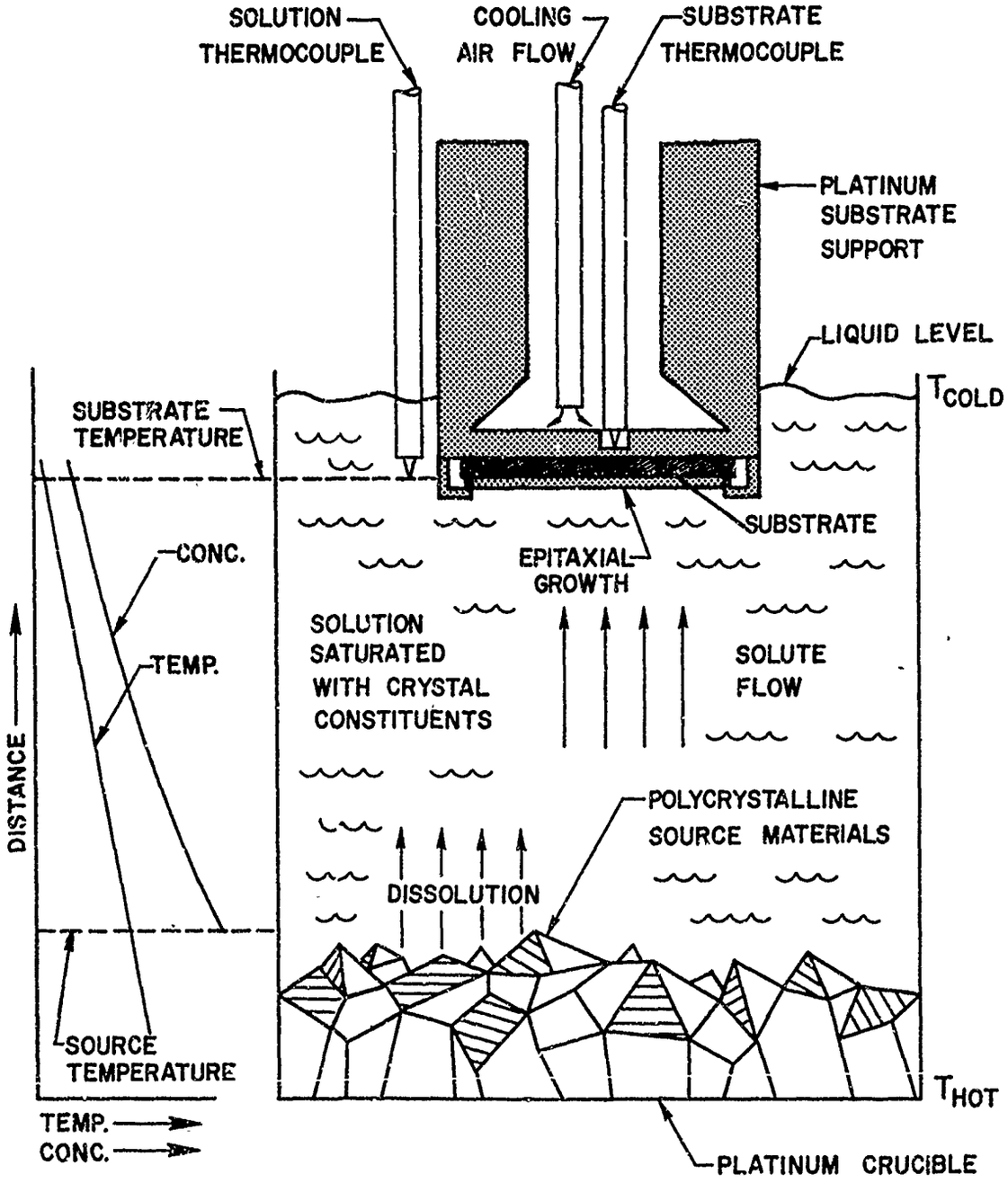

Figure 2. Steady-State Liquid Phase Epitaxial Growth Apparatus.

such as $Gd_3Ga_5O_{12}$, $Sm_3Ga_5O_{12}$ or $Nd_3Ga_5O_{12}$ for the uniaxial garnets, are congruently melting and can be produced by conventional Czochralski crystal growth.

The advantages of epitaxial growth include a higher degree of crystalline perfection than heretofore obtainable and an as-grown geometry which is ideal for device use, that is, very thin ($\sim$ 5-75μ) platelets already mounted on substrates for easy handling. The growth time is very short compared to conventional bulk growth techniques and high quality, large area thin films can be grown in a matter of minutes.

The recent successful LPE growth of garnet films with mobile magnetic bubbles in this laboratory and elsewhere[12] points out the advantages and capabilities of this technique for preparing uniaxial rare earth garnet thin films of device quality.

2.1.3. Substrate Selection.

A primary substrate consideration is its relative stability in the crystal growth solvent. To permit epitaxial growth of the magnetic material on the substrate and to minimize subsequent thermal strain or even catastrophic cracking, the lattice parameters and thermal expansion coefficients of the two materials must be very similar. The substrate must, of course, be nonmagnetic and perferably transparent to permit optical evaluation of the epitaxial layer.

Unfortunately the $YAlO_3$ used for epitaxial growth of $YFeO_3$ was rapidly attacked in a nonuniform fashion (see Figure 16) by the solvent, and proved unsuitable as a substrate. Lattice parameters of some of the pertinent garnets are shown in Table III and Figure 3. $Gd_3Ga_5O_{12}$ is sufficient for epitaxial growth

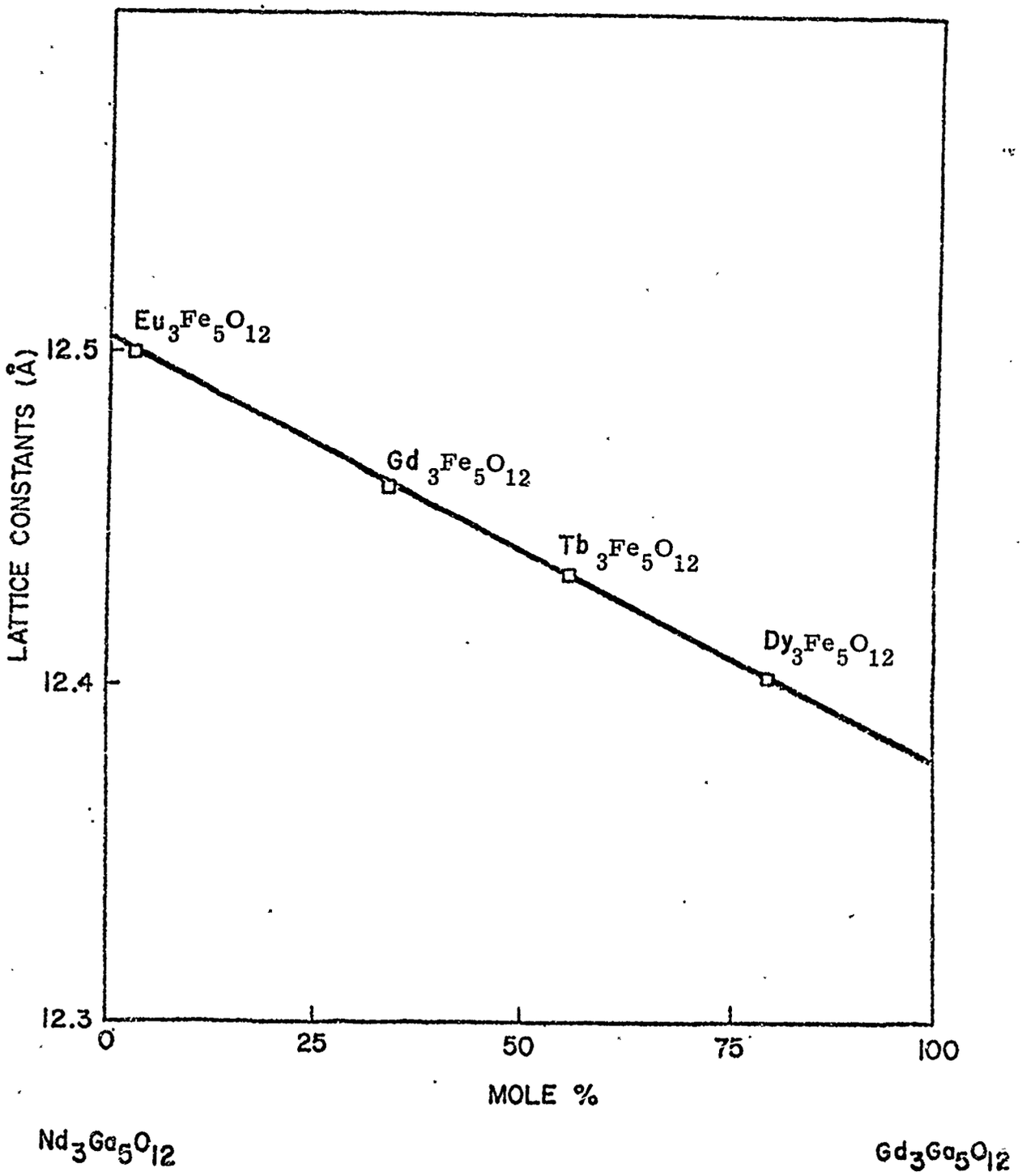

Figure 3. Lattice Parameter Match at ≈ 250°C
for Iron Garnets and Gallium Garnet Solid Solutions. (16)

of most of the lighter rare earth garnets. Recent results indicate that the distribution coefficients of nearly all the rare earth ions are sufficiently similar to permit controlled Czochralski growth of mixed garnet substrate materials,[16] permitting precise matching of the substrate lattice parameter (at least at room temperature) to the particular bubble garnet of interest. Typical lattice parameters are shown in Figure 3 for the case of mixed $Gd_3Ga_5O_{12}$-$Nd_3Ga_5O_{12}$ substrates. Room temperature matching does not ensure compatibility at growth temperatures due to differences in thermal expansion, and it is clear that much work remains to be done in this area. In view of these rapid advances in substrate preparation and LPE technology, the heteroepitaxial growth technique currently looks very promising.

2.1.4. Solvent Considerations

A review of a number of reports[15] of growth of magnetic rare earth materials by techniques using PbO-based solvents, as well as prior experimental work of our own, indicates that the PbO-based solvent has a number of inherent disadvantages, such as high volatility and reactivity toward the platinum crucible material at temperatures above 1000°C, higher density than the growing crystals causing them to float on the surface, and stability of other solid phases in addition to orthoferrites and garnets at temperatures below 1000°C. The first two difficulties can be alleviated in LPE growth by keeping the temperature below 1000°C at all times, and successful bubble garnet layers have been grown in this fashion.[12]

Problems associated with the PbO-based solvent may be largely circumvented by use of the $BaO-B_2O_3$ solvent system.[17] The advantages of this system are numerous: (1) there is very little corrosive attack on the platinum crucible material by the solvent, which permits at elevated temperatures (a) very long growth runs to be carried out, (b) several runs to be carried out using the same solution, and (c) minimization of the amount of platinum in solution which might be incorporated by the crystal. (2) the loss by vaporization of the BaO-based solvent is negligible. This is important for LPE growth, since it allows growth without a change in the liquid level. (3) The solubility of magnetic rare earth compounds is high and the viscosity of the solution is lower than in the PbO-based solvents.[18] Both of these factors enhance mass transport of crystal constituents in the solution from source to growing crystal. (4) The solution is less dense than the crystal, and thus the source material rests on the bottom of the crucible where it cannot interfere with the growth of the crystal. This is an important asset for epitaxial growth. (5) The ratio of distribution coefficients of gallium to iron is nearly unity, which permits close stoichiometry control during crystal growth of mixed gallium and iron garnets.

The only significant disadvantage of the most commonly used $BaO-B_2O_3$ composition is that its melting point is $\sim 915°C$,[18] as shown in Figure 4, several hundred degrees higher than the PbO-based solvent.

Although the uniaxial magnetic rare earth compounds can be grown from this eutectic $BaO-B_2O_3$ mixture, it is advantageous to reduce

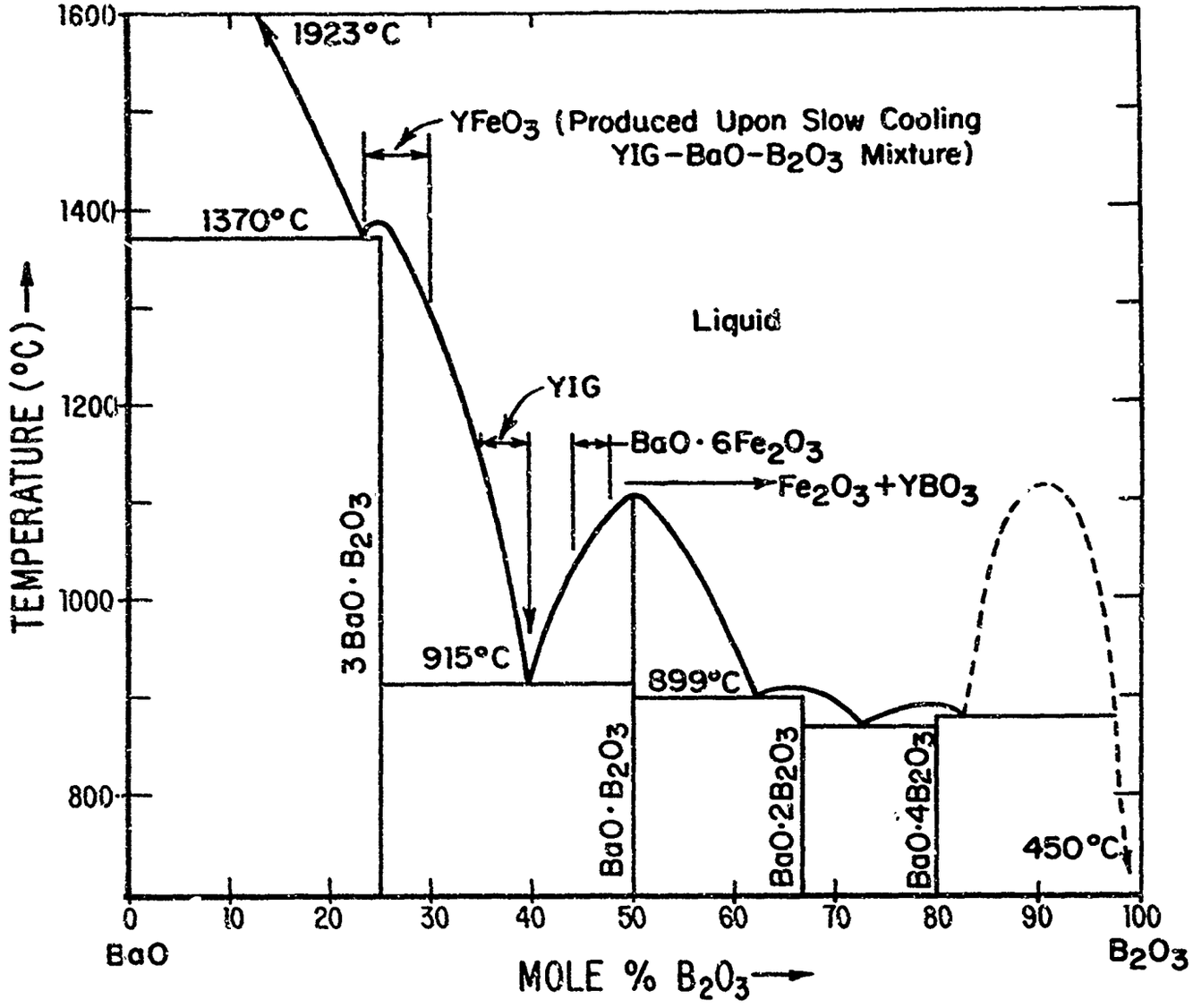

Figure 4. $BaO-B_2O_3$ Phase Diagram Depicting Solution Growth Stability Regions for Various Magnetic Materials.[17]

the melting temperature as much as possible for liquid phase epitaxial growth. For this reason, it was decided to examine possible additions to the $BaO-B_2O_3$ solvent which would make it more amenable to the crystal growth of $YFeO_3$ as well as the magnetic rare earth garnets. One such addition is BaF_2, which allows the melting range of the solvent to be shifted to lower values, and also appears to decrease the viscosity of the solvent. It is particularly advantageous to provide F^- in the melt because it has been noted [19] in the growth of $YFeO_3$ that PbF_2 added to the PbO-based melts enhances the growth of large single crystals containing fewer crystalline defects. BaF_2 has a very low vapor pressure at crystal growth temperatures, [20] and therefore, the stability of the solvent is unimpaired. An experimental program has been conducted to characterize the $BaO-B_2O_3-BaF_2$ ternary system in order to determine the optimum regions for crystal growth.

2.1.4.1. Interface Stability Analysis

It is appropriate to consider the maximum rate of growth that one may expect in crystals grown from this solution while still maintaining a planar interface. It is well-established that the cores of solution-grown orthoferrites and garnets often contain inclusions and growth faults [21,22] which are indicative of dendritic growth caused by an excessive growth velocity. A high quality single crystal, free from inclusions and inhomogeneities, requires a stable planar interface during growth. An estimate of the maximum velocity beyond which a planar interface will break down into a cellular interface can be obtained by a constitutional supercooling analysis. [23]

Such an analysis for the magnetic rare earth compounds in the solvent systems of interest shows that to avoid constitutional supercooling leading to interface breakdown and a dendritic mode of growth, the steady-state growth experiment should be designed for a growth velocity of $\sim 10^{-6}$-10^{-7} cm/s.[15]

This velocity is several orders of magnitude lower than the maximum allowable velocity during growth from a pure melt, but is comparable to values computed by Tiller[23] for solution growth of several classes of semiconductors from a binary solution (which range from 10^{-6} to 10^{-10} cm/s). It should be noted that V_{max} increases strongly as the growth temperature increases; and hence it is advantageous from this point of view to have the interface temperature as high as possible, commensurate with apparatus capabilities and other requirements.

However, there is another competing factor in LPE growth of the magnetic rare earth garnets, which requires growth as close to the maximum allowable velocity and at the lowest interface temperature as possible. for the following reasons. The best bubble garnet materials are thin (5-10μ) layers of $\{111\}$ orientation grown epitaxially on $\{111\}$ $Gd_3Ga_5O_{12}$ substrates. This type of growth is inherently nonequilibrium since the growth habit of bulk grown garnet crystals under nearly equilibrium conditions consists of $\{110\}$ and $\{112\}$facets. Thus there are crystallographic and kinetic constraints to retain the $\{111\}$ solid-liquid interface in the growing epitaxial layer balanced against a thermodynamic driving force to develop facets leading to $\{110\}$ and $\{112\}$ faces. Indeed

it has been found experimentally that the smoothest layers of epitaxial rare earth garnets are produced when the growth rates approach about 5μ in 20 minutes or an average interface velocity of $\sim 10^{-7}$ cm/s,[12] at average growth temperatures below 950°C. If the temperature is higher, it is energetically easier for the equilibrium facets to develop. If growth is much slower than this, the kinetic constraint is relaxed sufficiently to again permit equilibrium growth faces to appear, and the surface roughens with small growing garnet polycrystals exhibiting {110} and {112} faces. On the other hand, if growth is too rapid, the interface will retain its {111} orientation until an instability causes breakdown into cellular or dendritic morphology.

2.1.4.2. Fluid Motion Effects During Solution Crystal Growth.

Since convection in the liquid reduces the maximum allowable crystal growth velocity before interface breakdown,[23] it is of interest to characterize the growth solution with respect to convective instabilities caused by temperature gradients. There is a gravitational driving force for convective fluid motion whenever there is either a horizontal temperature gradient in the fluid or a vertical temperature gradient in which the upper portion is cooler than the lower. Both these conditions are present in the steady-state growth configuration described in Section 2.2 and it is desirable, therefore, to be able to control and minimize the degree of convective flow which occurs. Since the horizontal temperature gradient is negligible in our growth configuration, we shall direct our attention to an

analysis of the vertical gradient. Natural or cellular convection occurs when the vertical density gradient in the melt exceeds a critical value, governed by the existing temperature gradient and the temperature dependence of the fluid density. The critical temperature gradient beyond which cellular convection obtains is given by [24]

$$G_c = R_c \frac{\alpha_L \nu}{g \beta d^4} \tag{1}$$

where G_c = critical temperature gradient

α_L = thermal diffusivity in the liquid

ν = kinematic viscosity

g = gravitational consant

β = thermal expansion coefficient

R_c = critical Rayleigh number

d = depth of the liquid

We are interested in the variation of G_c with d for the $BaO\text{-}BaF_2\text{-}B_2O_3$ solution, for which

$\alpha_L \cong .02\ cm^2/sec$	(estimated value for oxides)
$\nu \sim .02$ gm-cm/sec	(estimated by comparison to experimental value for PbO solution)
$g = 980\ cm/sec^2$	
$\beta \sim 10^{-5}\ °C^{-1}$	(measured experimentally)
$R_c \sim 1770$	

A plot of G_c as a function of d is seen in Figure 5, where it is shown that the liquid depth must be kept below 2 cm to obtain a quiescent melt for a temperature gradient in excess of 2 °C/cm.

The convective flow causes an oscillating interface temperature which, even though it may not be great enough to drive the interface to an unstable growth mode, still may cause undesirable growth striations and inclusions in the crystal. Choice of experimental conditions should reflect this design criterion.

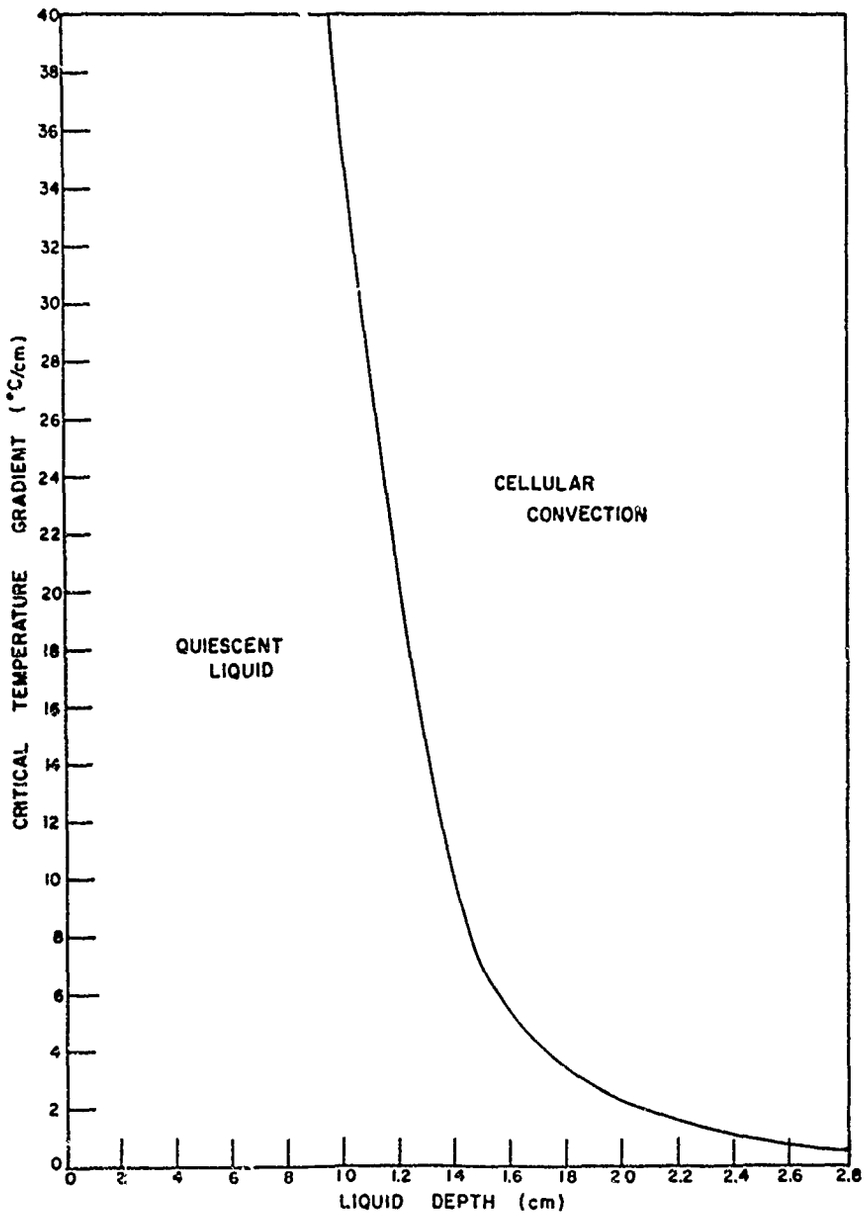

Figure 5. Convective Stability Regime for $BaO-B_2O_3-BaF_2$ Solvent in a Vertical Temperature Gradient.

(Calculated from equation 1)

2.2. Experimental Procedures.

2.2.1. Apparatus.

A steady-state crystal growth system suitable for the growth of magnetic rare earth compounds was constructed in the initial phase of this program. The system was designed to be capable of both bulk and hetero-epitaxial crystal growth.

Features of the system include, (1) a controlled thermal environment, (2) a stirring mechanism, (3) a means of changing the level of the seed during growth to permit precise time control for growth on the seed. (4) a large liquid surface exposure which provides the capability of growing on a large surface area seed; and (5) an air-cooled substrate support which provides additional control over the temperature of the substrate and a means for removing the heat of crystallization. These last two features are especially advantageous for epitaxial growth. The apparatus is illustrated in Figure 6.

2.2.2. Preparation of Seeds and Substrates.

2.2.2.1. Growth of $YFeO_3$ Seed Crystals for Steady-State Bulk Growth.

The method of growth of seed crystals required for the steady-state solution bulk growth was similar to that outlined by Wanklyn.[25] The crystal constituents were dissolved in a $PbO-PbF_2-B_2O_3$ solvent at approximately 1280°C and slowly cooled at a rate of 2°C/hr to nucleate and grow crystals of $YFeO_3$. The crystals grown by this method were nearly cubic, typically measuring 3-4 mm on a side and were quite suitable for use

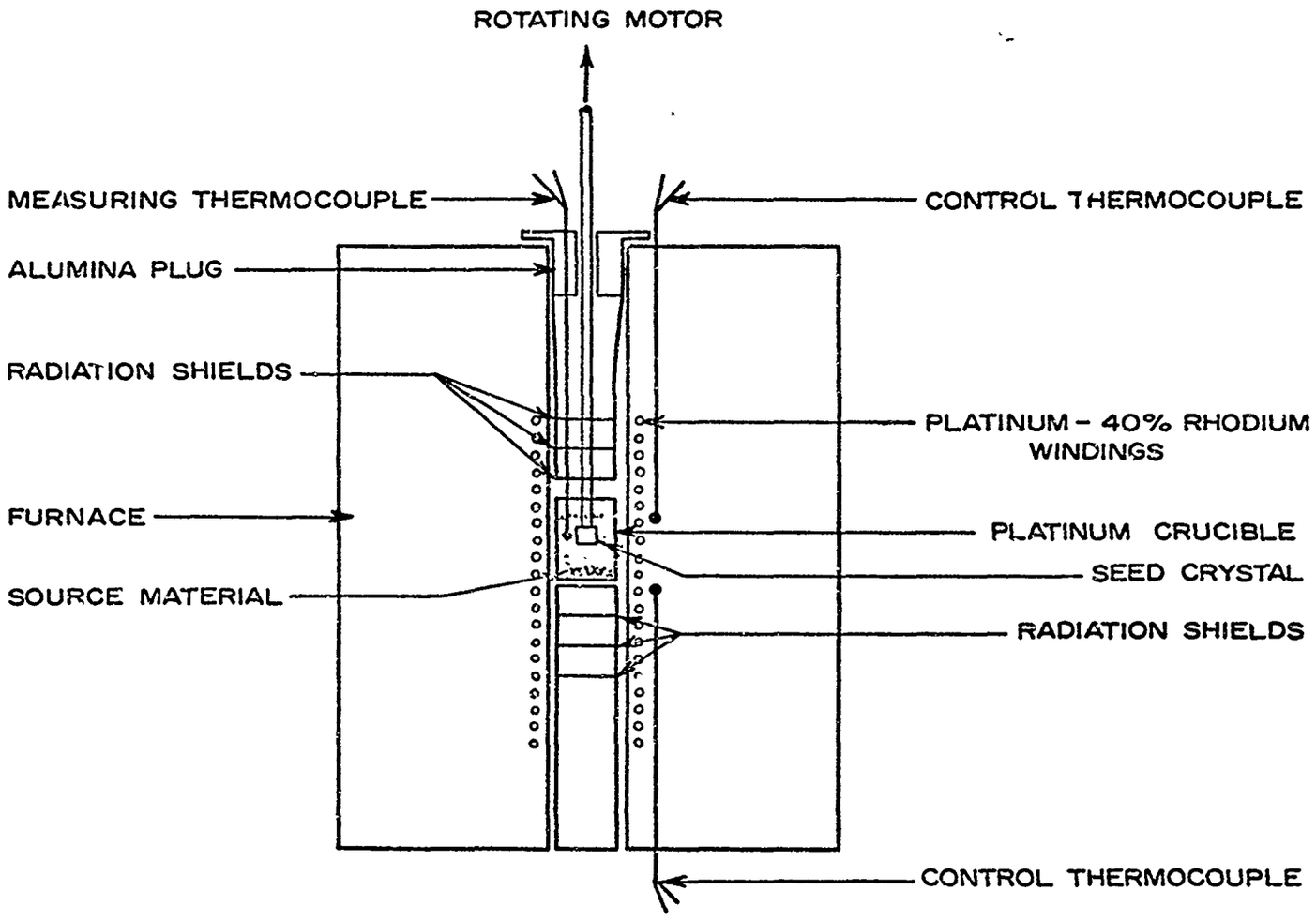

Figure 6. Schematic of Steady-State Crystal Growth System.

as seed crystals. There were, however, a number of voids and inclusions in these crystals which limited the useful areas to dimensions of approximately 3 mm x 3 mm.

2.2.2.2. Substrate Preparation and Evaluation.

The substrates used in the heteroepitaxial growth of $YFeO_3$ and the rare earth garnets were $YAlO_3$ and $Gd_3Ga_5O_{12}$, respectively, since these substrate materials were both commercially available and matched the lattice parameters of the crystals. A typical $Gd_3Ga_5O_{12}$ substrate used in heteroepitaxial growth of mixed magnetic garnets is shown in Figure 7. This substrate has been sliced from a Czochralski grown boule, lapped, prepolished with 1 micron diamond slurry, and polished by the Syton process.

Substrates used for successful epitaxial growth must be of very high quality. Indeed, when epitaxial layers were grown on defective substrates, the defects were propagated into the growing crystal. These defects in substrates which affect the growth of epitaxial magnetic material stem from two sources; those originating from imperfections in the bulk material from which the substrates are processed, and those originating from incomplete removal of mechanical surface damage during processing of the substrates. Imperfections in the bulk material available to date consist primarily of dislocations and inclusions. Mechanical surface damage results from cutting the bulk material into slices, lapping and prepolishing the slices with each step leaving less damage than the preceding. It has been found in this laboratory that several microns of material (the exact

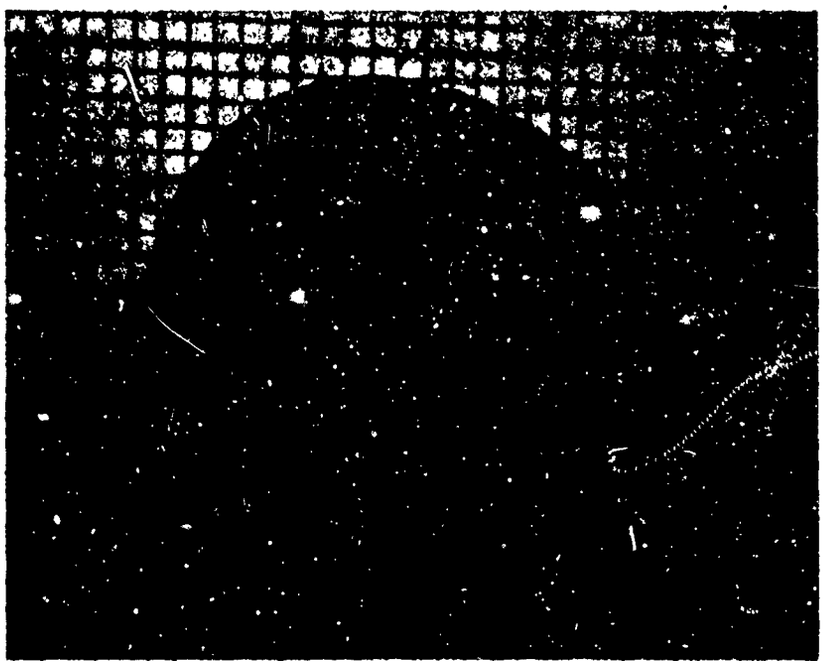

Figure 7. $Gd_3Ga_5O_{12}$ Substrate Material (Sliced and Polished). Millimeter Grid.

depth depends on the amount of damage caused in earlier steps and varies somewhat for each process) must be removed from a prepolished $Gd_3Ga_5O_{12}$ substrate to leave a damage-free surface. One way to do this is to use a chemical polishing process similar to that developed in this laboratory[15] and elsewhere[26] for $YFeO_3$. Further work with this technique in our laboratory has demonstrated that hot H_3PO_4 will chemically polish $YAlO_3$ in 2 minutes at 500°C and $Gd_3Ga_5O_{12}$ in 30 seconds at 320°C. In the case of $YAlO_3$, the removal rate is 3.75μm/minute and for $Gd_3Ga_5O_{12}$ it is 14μm/minute. However, a more effective technique has been to remove the material by using the Syton process. A typical removal rate(for particular conditions of substrate size, slurry flow rate, loading and surface velocity) for the Syton polishing procedure has been determined to be approximately 3.4μm/hr for $Gd_3Ga_5O_{12}$.

To ascertain the quality of the finished substrate surface, any residual defects can be exposed by selectively etching the substrate. This has been accomplished on (111) faces for $Gd_3Ga_5O_{12}$ substrates by etching them in H_3PO_4 at approximately 160°C for a period of twenty minutes. As shown in Figure 8, this technique has been used to expose mechanical damage left from scratches which had been only partially removed by Syton polishing, growth striations and dislocations.

Figure 8a. Dislocation Etch Pit Patterns in Syton Polisi.ed {111} $Gd_3Ga_5O_{12}$ which has been Etched in 160°C H_3PO_4 for 20 minutes (100 X)

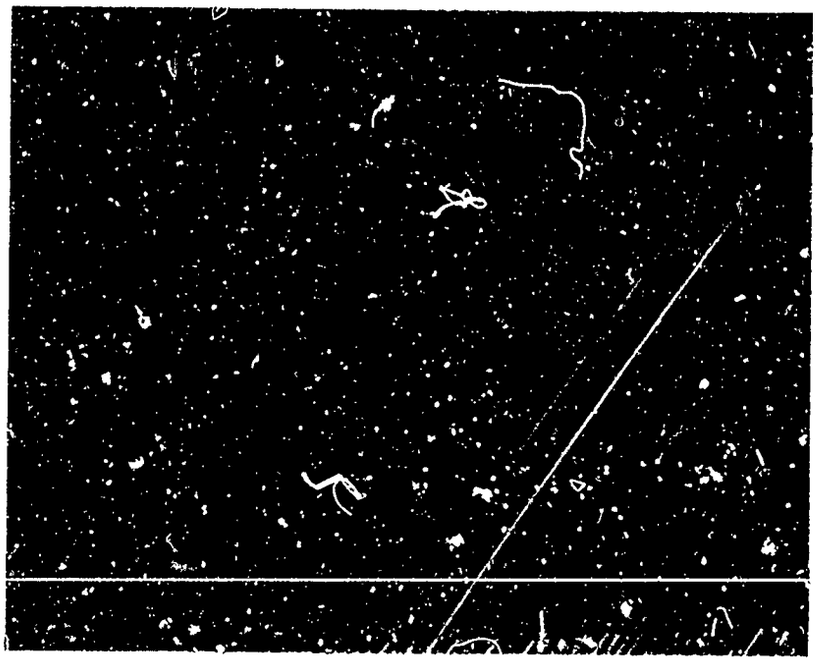

Figure 8b. Growth Striations in a Different Syton Polished {111} $Gd_3Ga_5C_{12}$ Subatrate which has been Etched in 160°C H_3PO_4 for 20 Minutes. (200 X)

2.2.3. Characterization of the $BaO-B_2O_3-BaF_2$ Solvent.

2.2.3.1. Liquidus Surface and Solubility of $YFeO_3$ and Rare Earth Garnets.

In order to best exploit the advantages of the BaO-based solvents, the ternary system obtained by adding BaF_2 to the BaO-39.5 mole % B_2O_3 eutectic mixture was investigated. As BaF_2 is added, the liquidus point becomes a curve in the ternary diagram as shown in Figure 9. The experimental points in this diagram were determined by continuously monitoring the temperature of a solvent melt of known composition, and noting the temperature at which a Pt wire inserted in the melt could no longer be moved freely, indicating a very rapid increase in viscosity. The experiments were conducted in a muffle furnace, and once a reasonably low melting composition was found (such as 41 mole % BaO, 41 mole % B_2O_3, 18 mole % BaF_2), solubility determinations of $YFeO_3$ were conducted in the same furnace. Here, small crystals of $YFeO_3$ were suspended by a platinum wire in the nearly saturated melt, held for several hours, removed and examined optically. Either (1) the solution was unsaturated and the crystal dissolved or developed rounded corners, or (2) the solution was supersaturated and the crystal grew, as did a myriad of smaller crystals which nucleated both on the seed and on the platinum wire. The solubility curve obtained in this fashion is shown in Figure 10. The data can be fitted to an equation of the form

$$x = x_o e^{-\Delta H/RT} \quad , \qquad (2)$$

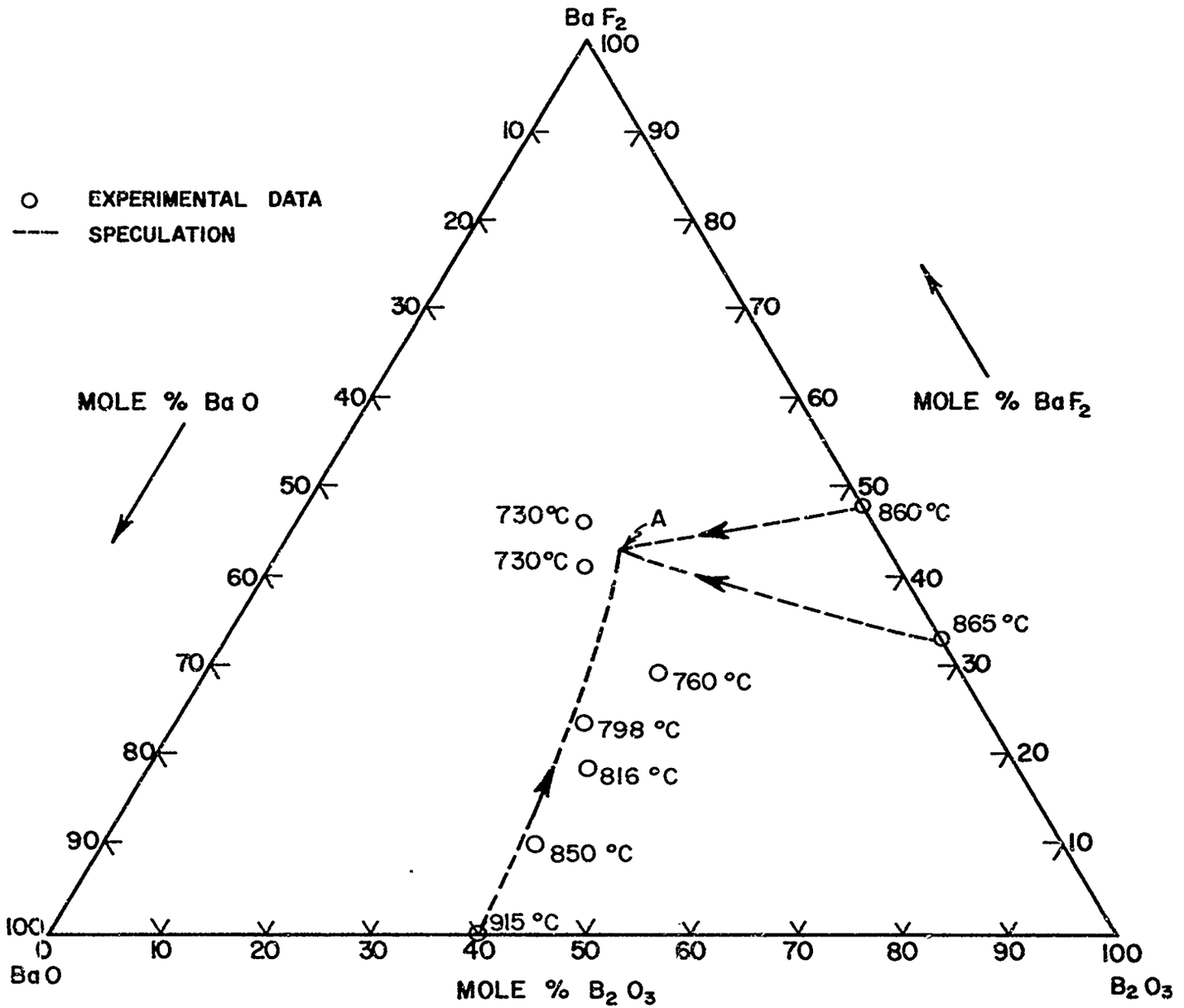

Figure 9. Possible Partial Liquidus Projection for $BaO-B_2O_3-BaF_2$ System with a Ternary Eutectic at A. (Schematic only.)

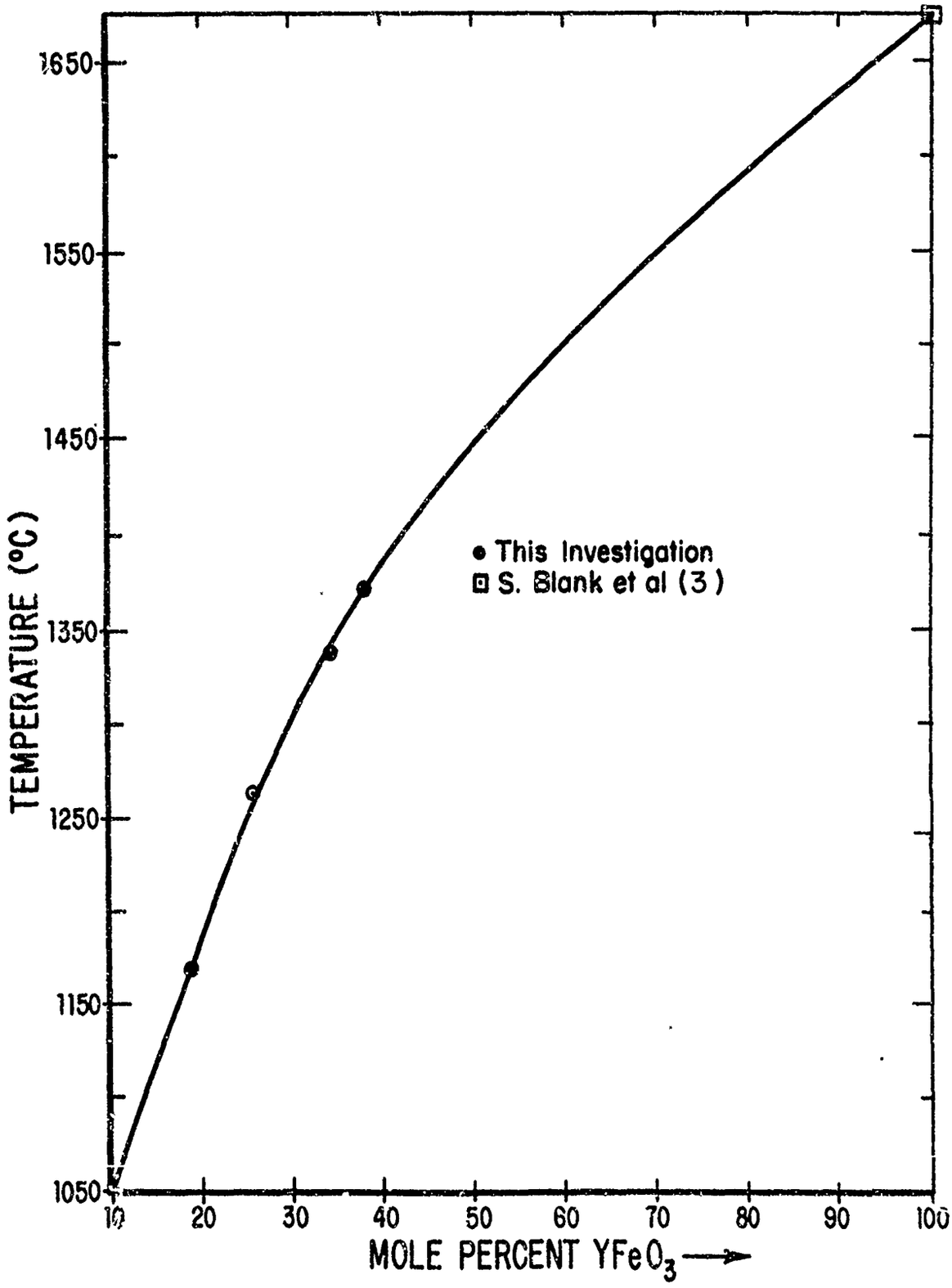

Figure 10. Solubility Curve for $YFeO_3$ in 41 (Mole) % BaO, 41% B_2O_3, 18 % BaF_2.

where x = mole fraction $YFeO_3$,

x_o = constant,

ΔH = activation energy (cal/mole),

R = gas constant, and

T = temperature (°K).

Here x_o = 5.03 and ΔH = 19,408 are assumed constant over a fairly wide range of temperature.

The liquidus surface of the rare earth garnet solution was estimated by suspending a $Gd_3Ga_5O_{12}$ substrate in the solution, systematically varying temperature and concentration of the solution, and noting (after removal from the furnace and subsequent cleaning) the values at which appreciable attack of the substrate occurred instead of epitaxial growth on the substrate. The data obtained in this fashion (only approximate since the $Gd_3Ga_5O_{12}$ is never in true equilibrium with the solution) are shown in Figure 11.

2.2.3.2. Densities of the Crystal Growth Solutions.

The densities of the solutions were determined experimentally with the aid of a recording electrobalance. Using this technique, a Pt bob ~5 mm in diameter was suspended from a Pt wire, and its weight first recorded as a function of temperature from 1000-1200°C while it hung just above the melt. Then it was inserted into the solution and its apparent weight recorded once again as a function of temperature. The surface tension effect exerted by the solution upon the suspension wire was measured by repeating the experiment without the bob. Density is given by[27]

$$\rho = \frac{B + S}{V + v} \qquad (3)$$

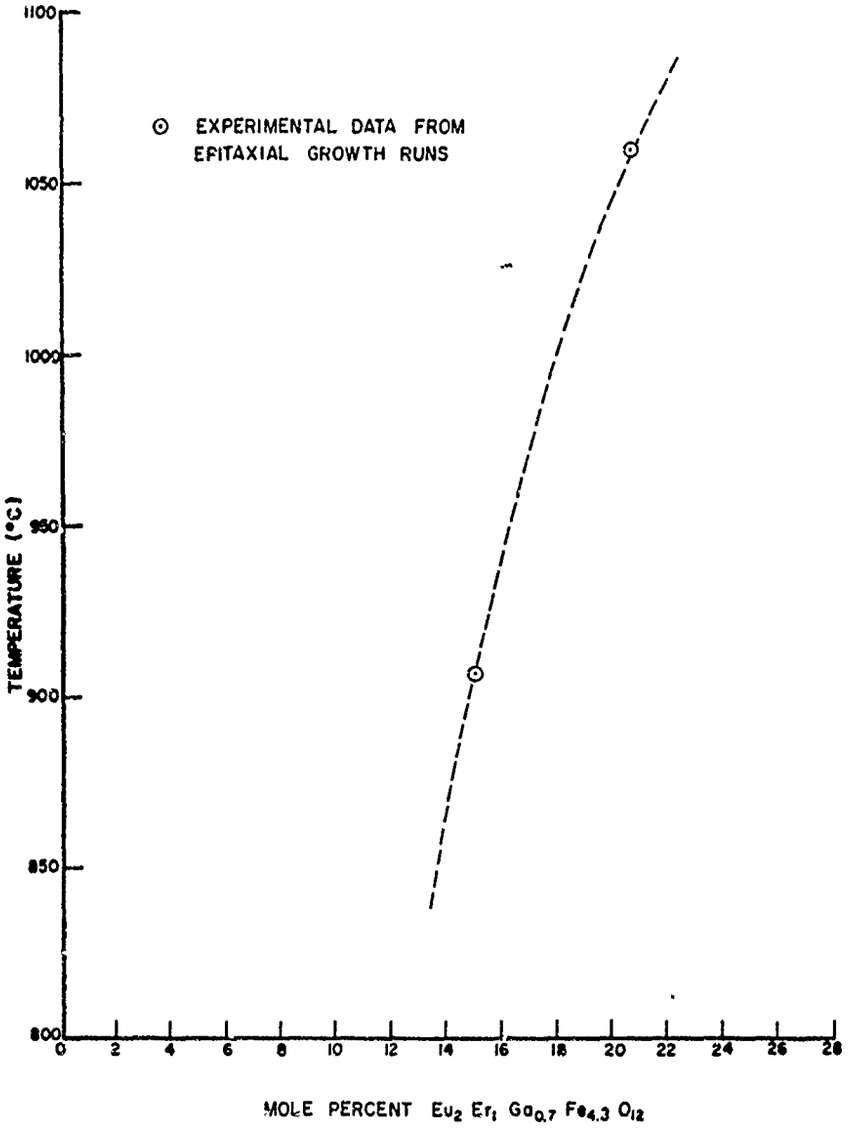

Figure 11. Tentative Solubility Curve for $Eu_2Er_1Ga_{0.7}Fe_{4.3}O_{12}$ in the BaO-based Solvent.
The curve drawn between the data points is schematic only.

where ρ = density,

B = difference in weight of bob + immersed suspension in air and in the melt,

S = surface tension effect,

V°= volume of bob, and

v = volume of immersed suspension ($v << V°$).

The density of the pure $BaO\text{-}B_2O_3\text{-}BaF_2$ solvent as well as solutions of garnet and orthoferrite in this solvent are shown in Figure 12. The thermal expansion coefficient of the solution is given by[27]

$$a = \frac{1}{\rho}\left(\frac{\partial \rho}{\partial T}\right)_p \qquad (4)$$

and was found to be between 5×10^{-5} and 1.11×10^{-4} for all the solutions of interest.

The concentration dependence of the density is shown for garnet solutions in Figure 13. The curvature is a measure of the partial molar volume of the garnet in the solvent (if it is assumed to exist as a discrete entity) and again shows that the solute is not an ideal thermodynamic solution at these temperatures.

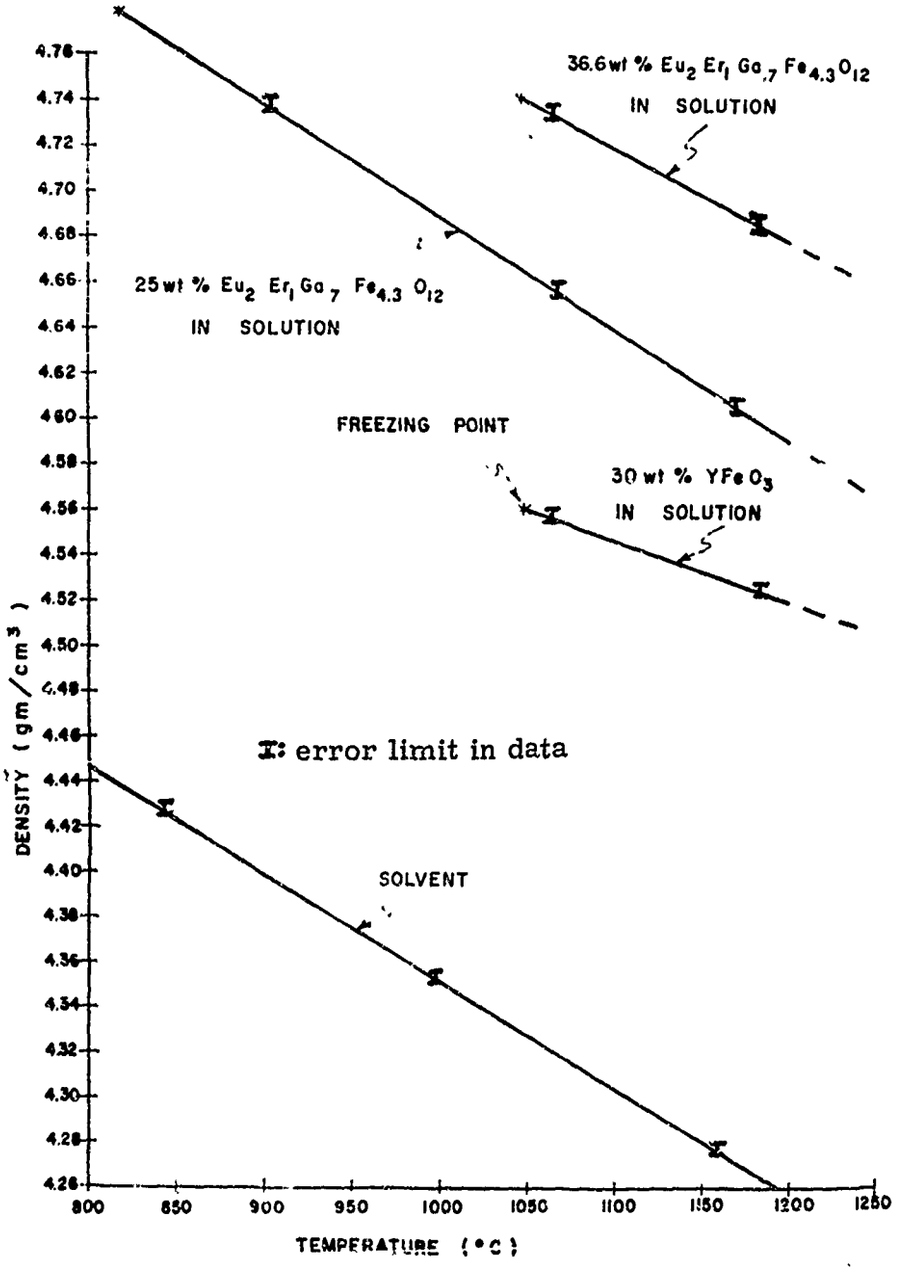

Figure 12. Temperature Dependence of the Density of Various Crystal Growth Solutions: Solvent Composition 41 (mole)% BaO, 41% B_2O_3 18% BaF_2.

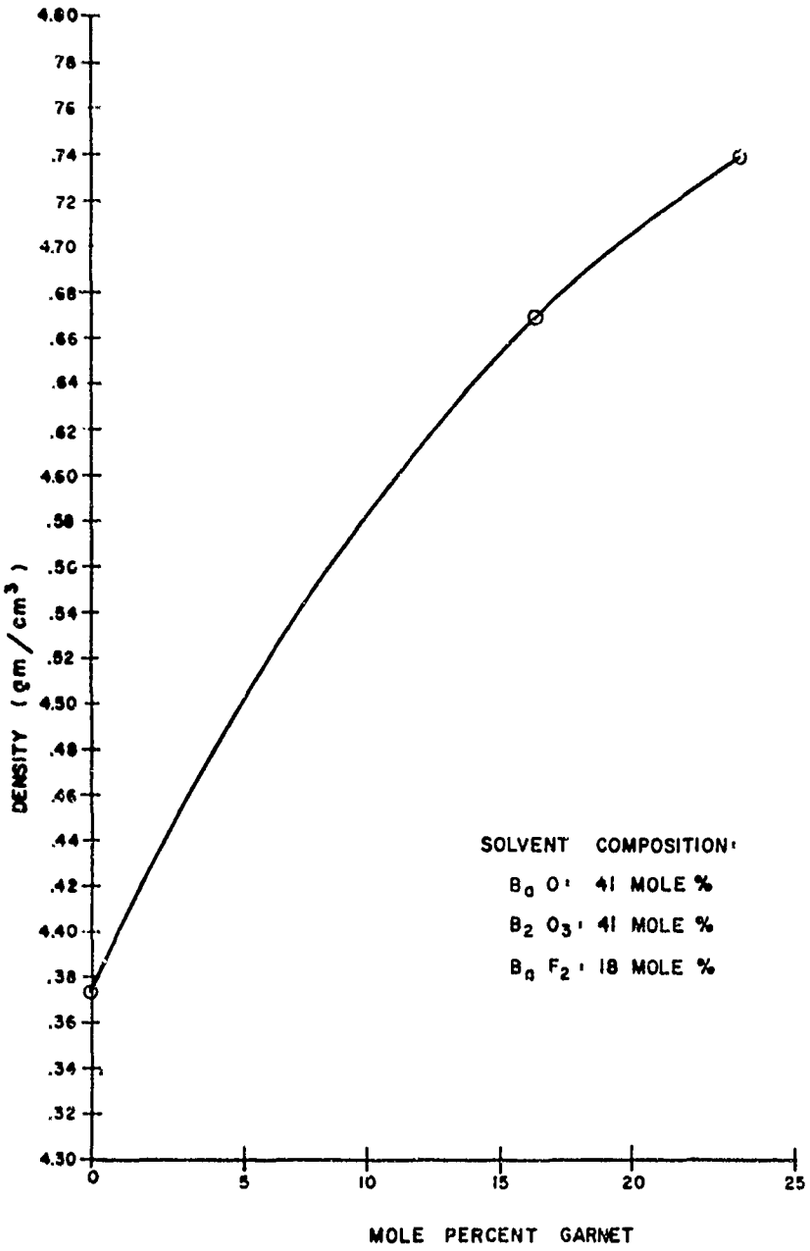

Figure 13. Concentration Dependence of the Density for $Eu_2Er_1Ga_{0.7}Fe_{4.3}O_{12}$ in the BaO-Based Solvent. (Temperature = 1050°C)

2.2.4. Steady-State Crystal Growth.

2.2.4.1. Orthoferrites.

2.2.4.1.1. Procedure.

The procedures for bulk and heteroepitaxial $YFeO_3$ growth experiments were similar. The materials used were from various suppliers and have the following quoted purity levels: Y_2O_3, B_2O_3 and Fe_2O_3-99.999%; BaF_2-99.9%. BaO was obtained from $BaCO_3$, which was 99.999% pure.

The polycrystalline source material was prepared from the Y_2O_3 and Fe_2O_3 powders, which were pressed into a 3/8" diameter pellet die. The pressed pellets were then sintered at 1225°C for 20 hours in air, ground, repelleted and fired again at 1300°C for 48 hours. X-ray powder diffraction analysis indicated that all but approximately 5% of the starting materials had reacted to form $YFeO_3$. Emission spectrographic analysis showed the pellets to contain less than 50 ppm impurities. The apparent density was 53% of the theoretical density for $YFeO_3$.

A solution saturated with $YFeO_3$ was mixed, loaded into a platinum crucible and the $YFeO_3$ source material was then added. A seed crystal was mounted on the end of a rod which could rotate the seed continuously in the solution. In all these runs, the seed crystal was oriented so that the c-axis was parallel to the axis of rotation. For the epitaxial growth runs, the substrate was mounted on an air-cooled support. The growth parameters for these runs are listed in Tables IV and V.

TABLE IV

Parameters for Seeded, Steady-State Growth Runs of $YFeO_3$

Composition of Solvent (mole percent) BaO B_2O_3 BaF_2	Seed Temperature (°C)	Source-Seed Temperature Gradient (°C/cm)	Rotation Rate (rpm)	Run Time (Hours)	Remarks*
53.4 35.6 11.1	1112	3.9	22	46	150μm of growth; growth rate $\sim 9.5 \times 10^{-8}$ cm/s
53.4 35.6 11.1	1115	7.6	50	168	Spontaneously nucleated polycrystalline growth
53.4 35.6 11.1	1110	3.4	50	235	500 μm of growth; growth rate $\sim 5.9 \times 10^{-8}$ cm/s
42.6 41.0 16.4	1302	0.19	25	260	Limited nucleation on stirring rod; crystals grew to 4mm x 3mm x 3mm
42.6 41.0 16.4	1302	0.38	25	189	Spontaneous nucleation-stepped polycrystalline growth
43.4 40.4 16.2	1307	0.14	25	109	390μm of growth; growth rate $\sim 8.7 \times 10^{-8}$ cm/s

* See text for further discussion of the results.

TABLE V

Growth Parameters for Heteroepitaxial $YFeO_3$ Runs on $YAlO_3$ Substrates in the Steady-State System

Composition of Solvent (mole percent) BaO	B_2O_3	BaF_2	Substrate Temperature (°C)	Source-Substrate Temperature Gradient (°C/cm)	Run Time (Hours)	Remarks*
43.4	40.4	16.2	1292	0.152	6.5	Substrate dissolved
43.4	40.4	16.2	1288	1.17	5.3	Severe solvent attack on substrate
43.4	40.4	16.2	1178	2.78	0.50	Severe solvent attack on substrate
43.4	40.4	16.2	1070	2.61	0.50	Growth occurred as shown in Figure 16
43.4	40.4	16.2	1065	4.25	0.17	Growth layer was more continuous than 1070°C run, but was still not epitaxial
43.4	40.4	16.2	1053	6.22	0.17	Growth layer was more continuous than 1070°C run, but was still not epitaxial

* See Section 2.2.4.1.3 for further discussion of the results.

2.2.4.1.2. Results and Discussion of Bulk Steady-State Growth.

During the course of this series of experiments the growth parameters were systematically changed in each successive run in order to determine optimum growth conditions. To keep the time required to a minimum, the growth runs were all relatively short and this was reflected in the amount of growth obtained.

$YFeO_3$ was successfully grown onto seed crystals in two different temperature ranges--the lower one was at approximately 1110°C and the upper one was approximately 1300°C. Microscopic examination and Laue X-ray diffraction patterns showed that the new growth had the same orientation as the seed.

The steady-state growth in these runs ranged from 300-500 μm thick. The approximate growth rates were 7.7×10^{-8} cm/s and 2.0×10^{-7} cm/s for growth temperatures of 1110°C and 1300°C respectively. In general, examination of cross sectional areas showed that although the original seed contained a number of inclusions, the new growth contained significantly fewer.

The surface morphology of crystals grown in the low temperature range (1110°C) was rather rough, having formed some steps and a dull surface finish. However, the higher temperature growth (1300°C) yielded crystals having very good morphology with a well defined pseudo cubic habit common for the orthoferrites, well shaped facets and specular surfaces.

In most runs, crystals also nucleated and grew on the rod supporting the seed crystal. Some of these crystals, from the high temperature runs, grew to a size of 4mm x 3mm x 3mm and although the cores contained a

number of inclusions, high quality slices (i.e., slices having no voids, grain boundaries or twin planes measuring 3mm x 3mm x 60μm)were processed from these crystals as shown in Figure 14.

The principal difficulty encountered in the steady-state growth was spontaneous nucleation of small crystallites on the seed support rod and stirring blade. A minimum amount of this spontaneously nucleated growth was obtained using a source-seed temperature gradient of 0.14°C/cm. This temperature gradient was the lowest that could be reliably controlled, thus limiting attempts to reduce the degree of supersaturation by decreasing the temperature gradient.

Thin slices (approximately 2.5 mils thick) of the $YFeO_3$ crystals from the low-temperature (1110°C) runs containing portions of the steady-state growth and the original seed showed that the steady-state growth was nearly opaque to visible light. In contrast to this, the steady-state $YFeO_3$ growth in the high-temperature runs transmitted light as well as the seed on which it grew. This may be related to the amount of barium incorporated in the lattice of the material (0.082 and 0.015 wt. % for the low- and high-temperature growth, respectively, see Section 3.1).

A number of slices taken from crystals which spontaneously nucleated and grew on the seed crystal support rod have shown alternate light and dark regions which give a "picture frame" effect (Figure 15). These bands indicate that localized nonuniform growth conditions prevailed during growth. The

Figure 14. A Slice of $YFeO_3$ Processed from a Crystal Grown in the Steady-State System from a BaO-based Solvent. It is Shown here Containing a Serpentine Magnetic Domain Pattern; the Scratches Occurred During Handling. (31X)

Figure 15. Platelet of $YFeO_3$ Showing Banded Pattern. The Irregularly Shaped Holes Stem from Dissolving Solvent out of Inclusions. (31X)

details of the origin and nature of these dark regions are not yet well established. Similar banding observed in crystals grown from PbO-based solvents has been attributed to variations in Pb content.[22] Wood et. al.[28] have suggested that for the rare earth orthoferrites containing lead, the light absorbed at a wavelength of $\sim 0.7\mu$ in these materials may be due to the presence of Fe^{4+} ions.

2.2.4.1.3. Results and Discussion of Heteroepitaxial $YFeO_3$ Growth Experiments.

Typical growth parameters used in this series of experiments are listed in Table V. The best results in these experiments were obtained using a substrate temperature of 1070°C and a source substrate temperature gradient of 2.6°C/cm. Under these conditions, oriented polycrystalline $YFeO_3$ grew, but there was an intermediate layer between the $YAlO_3$ substrate and the $YFeO_3$. Electron microprobe analysis of this intermediate layer showed that it contained a mixture of yttrium, aluminum, iron and oxygen.

The $YFeO_3$ which deposited onto the intermediate layer had grown in the form of small, closely-spaced rectangular faced blocks measuring 50-80 μm along an edge as shown in Figure 16. A microscopic examination of a cleaved crystal, displaying the cross-sectional area of the $YAlO_3$ substrate with the new growth on it, showed that the substrate had been attacked by the growth solution leaving a very rough substrate surface on which the intermediate layer and $YFeO_3$ grew. This substrate attack is also shown in Figure 16 where part of the growth has fallen off.

For substrate temperatures above 1070°C, the substrate attack was so severe that little or no growth took place. The lower temperature runs deposited layers of material on the substrate, but the layers

did not adhere to the substrate while removing the solidified growth solution in dilute acid. Similar attack of $YAlO_3$ substrates were noted by investigators using PbO-based solvents.[29]

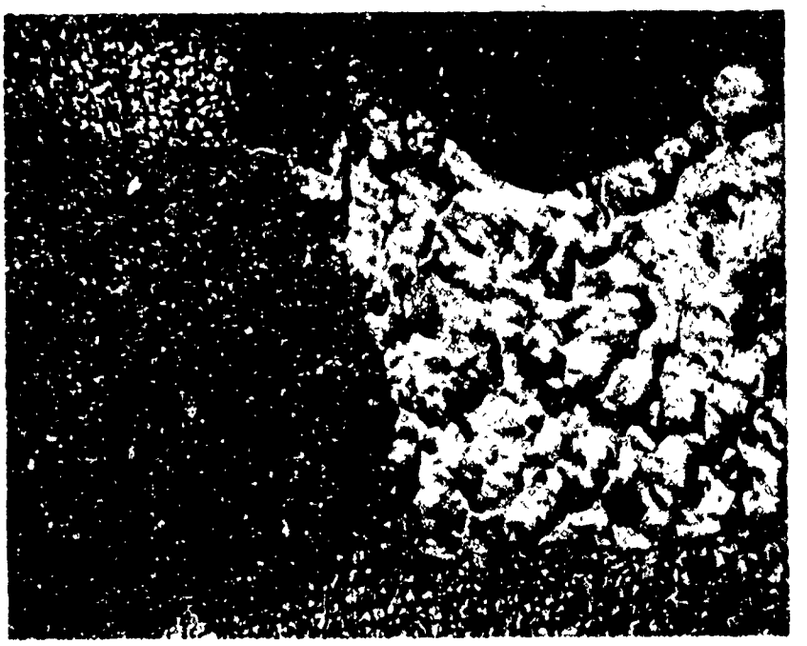

Figure 16. Results of Attempted Heteroepitaxial Growth of $YFeO_3$ on an $YAlO_3$ Substrate. Left Portion is $YFeO_3$; Right Portion is Substrate Surface which has been Attacked by Growth Solution. (100X)

2.2.4.2. Heteroepitaxial Growth of the Rare Earth Garnets

Studies of liquid phase epitaxial growth were made using both the BaO-based solvent, which contains 41 mole % BaO, 41% B_2O_3, 18% BaF_2, as well as a PbO-based solvent, containing 94 mole % PbO, 6% B_2O_3. As mentioned in Section 2.1.4, some of the disadvantages inherent in high temperature bulk crystal growth in the $PbO-B_2O_3$ solvent, such as its very high reactivity and volatility, are alleviated at the relatively low LPE growth temperature range of 800-1000°C. Hence, a critical experimental re-evaluation of the relative merits of each solvent is necessary at these temperatures, even though the BaO-based solvent was demonstrated to be advantageous in the 1000-1300°C temperature regime necessary for bulk solution growth.[15]

The garnet chosen for the initial LPE growth was $Eu_2Er_1Ga_{0.7}Fe_{4.3}O_{12}$, since it was grown successfully by Shick et al.[12] in the $PbO-B_2O_3$ solvent, and exhibits reasonable bubble mobility. In addition, its measured room temperature lattice parameter (12.406Å)[12] is fairly close to that of the measured lattice parameter of the $Gd_3Ga_5O_{12}$ substrate (12.384Å - see Section 3.2).

Preliminary growth runs were performed by rapidly cooling a saturated solution of the garnet in either $PbO-B_2O_3$ or $BaO-BaF_2-B_2O_3$ solvent contained in a Pt crucible set in a muffle furnace. The $Gd_3Ga_5O_{12}$ substrate was held just above the solution for five minutes to allow temperature equilibration, and then lowered into the solution as the furnace cooled at rates of 120-600°C per hour. Insertion temperature varied from 900-950°C, and the removal temperature ranged from 800-850°C . The proper starting

temperature was found by inserting the substrate systematically at various temperatures until the lowest temperature was found below which nucleation was so rapid that polycrystalline growth occurred instead of single crystal epitaxial growth. At temperatures higher than this there was a tendency for the solvent to begin etching the substrate surface nonuniformly, producing a bumpy surface, which then propagated into the epitaxial layer as shown in Figure 17a, b. At the lower temperature, the substrate (+ epitaxial growth) was quickly cooled to room temperature by pulling it out of the furnace, and then the remaining solvent was washed off with hot 20% HNO_3.

Exploratory LPE growth runs were also performed using a transient technique in which the BaO-based solution was supercooled to the substrate insertion temperature and held at that temperature while the substrate was cooled still further before lowering into the melt. A constant interface temperature was maintained by holding the substrate on a massive Pt block cooled on the back side by flowing air. The block also contained a thermocouple well to record substrate temperature. Best results were obtained when the substrate temperature was maintained initially about 40°C below the melt temperature of $\sim$ 980°C (at which temperature the solution was supercooled $\sim$ 62°C below the saturation temperature).

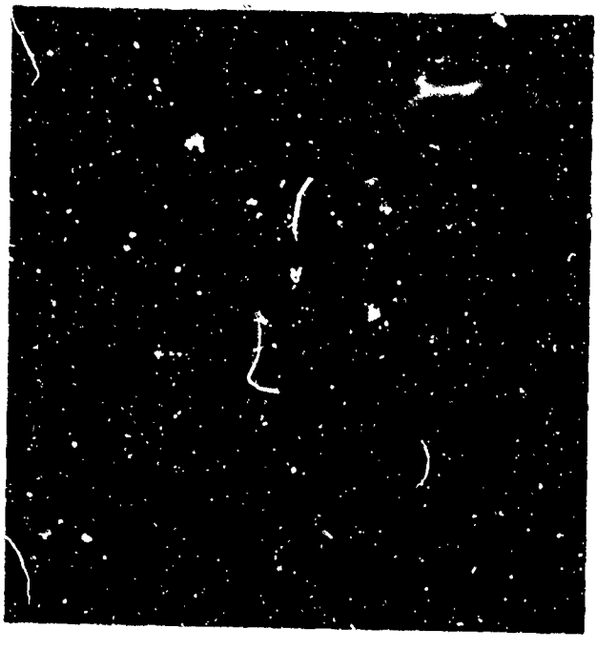

Figure 17a. {111} $Gd_3Ga_5O_{12}$ Substrate after Attack by $PbO\text{-}B_2O_3$ Solvent in only Slightly Supersaturated Solution at 900°C (19,000X).

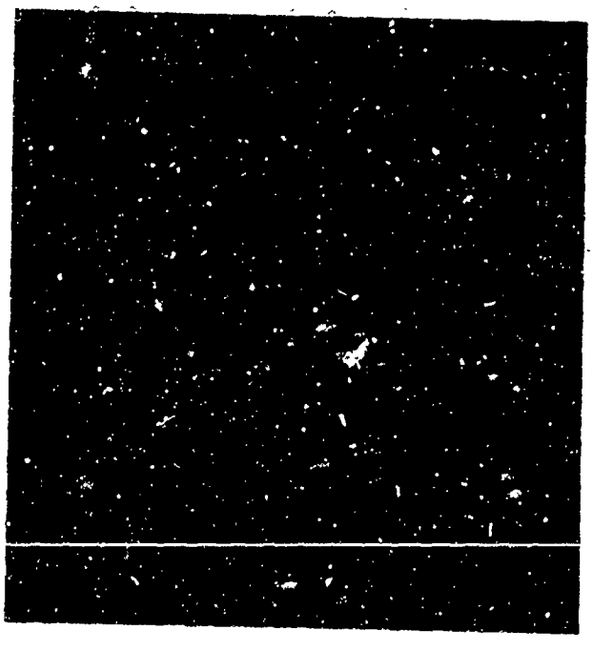

Figure 17b. Surface Morphology of $Eu_2Er_1Ga_{0.7}Fe_{4.3}O_{12}$ Epitaxial Layer which Grew upon This Rough Surface. (19,000X)

The compositions of the solutions used for the LPE growth runs were as follows:

(1) $PbO-B_2O_3$	Solvent	(2) $BaO-BaF_2-B_2O_3$	Solvent
PbO	90.01 gm	BaO	94.83 gm
B_2O_3	1.80	B_2O_3	42.92
Eu_2O_3	2.04	BaF_2	47.36
Er_2O_3	1.12	Eu_2O_3	12.60
Ga_2O_3	0.58	Er_2O_3	6.92
Fe_2O_3	5.00	Ga_2O_3	3.59
		Fe_2O_3	57.21

Using substrates prepared as described in Section 2.2.2.2., epitaxial layers 5-20 μm thick were grown exhibiting magnetic bubble domains by the transient technique as well as the steady-state technique in both the BaO-based and $PbO-B_2O_3$ solvents. Controlled high quality epitaxial growth necessitates a very smooth substrate finish. Any defects in the substrate, such as inclusions or scratches were readily propagated and enlarged in the epitaxial layer as shown in Figure 18.

The preliminary growth experiments indicated some differences between the PbO-based and BaO-based solvents. The epitaxial layer and substrates themselves have more of a tendency to crack in the BaO solvents as shown in Figure 19. The principal reason for this seems to be that the BaO-based solvent used in the initial growth runs was higher melting and, therefore, closer to its freezing point and more viscous at 800-900°C (although it is less viscous than the PbO-based solvents above 1000°C). Therefore, more of the solvent adhered

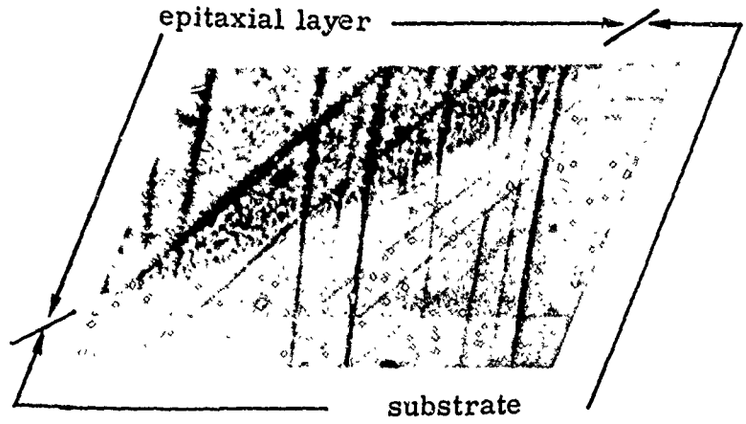

Figure 18. Top View of Epitaxial Layer of $Eu_2Er_1Ga_{0.7}Fe_{4.3}O_{12}$ on {111} $Gd_3Ga_5O_{12}$ Substrate Showing Small Scratches in Substrate Enlarged in the Epitaxial Layer. The Bare Substrate is a Region Upon Which the Epitaxial Layer Failed to Nucleate and Grow. (200X)

Figure 19. Crack Pattern in $Eu_2Er_1Ga_{0.7}Fe_{4.3}O_{12}$ Epitaxial Layer Grown on {111} $Gd_3Ga_5O_{12}$ Substrate in BaO-based Solvent. (200X)

to the layer as it was pulled out of the melt. The difference in thermal expansion coefficients between the solvent and the substrate epitaxial layer set up differential stresses exceeding the yield stress of the substrate if the solvent layer was thick enough. Observation of cracked substrate areas under thick regions of solvent and crack-free areas under thin regions substantiated this model. No such cracking occurred when the layers were grown in the PbO-based flux, even when a thick layer of solidified flux remained. Apparently the difference in thermal expansion was not as great in this system.

The color of the epitaxial layers differed depending upon the solvent used, brownish-green for those grown in the PbO-based solvent to a more translucent light lemon-green color for those grown in the BaO-based solvent. The causes of this color change are still being investigated but may be caused by the very low barium impurity content, $\sim$24 ppm Ba^{2+}, in epitaxial layers grown in the BaO-based solvent.

In general we have found, as noted by others,[12] that surface morphology improves at crystal growth temperatures below 1000°C, and that the $\{111\}$ growth rate must be constrained at $\sim 10^{-7}$ cm/s to prevent formation of equilibrium $\{110\}$ and $\{112\}$ facets at lower velocities, or cellular breakdown at higher velocities. Examples of some of these morphologies are shown in Figures 20a, b, c. Figure 21 shows the transition between a rough and smooth layer. The rough region lies at the edge of the substrate. Also shown is a typical triangular growth defect in this region.

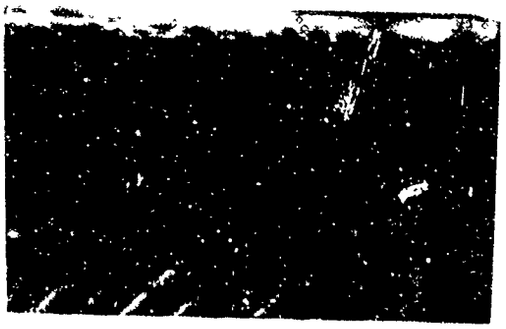

Figure 20a. Cross Section of $Eu_2Er_1Ga_{0.7}Fe_{4.3}O_{12}$ Epitaxial Layer on {111} $Gd_3Ga_5O_{12}$ substrate Showing Dendritic Breakdown after ~1 Micron of Growth. 6000X. (Apparent Roughness in Substrate is a Cleavage Artifact).

Figure 20b. $Eu_2Er_1Ga_{0.7}Fe_{4.3}O_{12}$ Epitaxial Layer Top Surface, Showing Breakdown of the Layer to the Equilibrium Habit.(1000X)

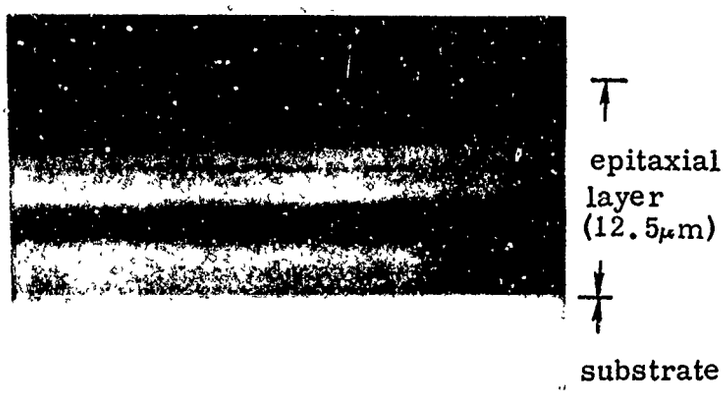

Figure 20c. Cross Section of $Eu_2Er_1Ga_{0.7}Fe_{4.3}O_{12}$ Epitaxial Layer on {111} $Gd_3Ga_5O_{12}$ Showing Uniform Growth and a Smooth Surface (2400X).

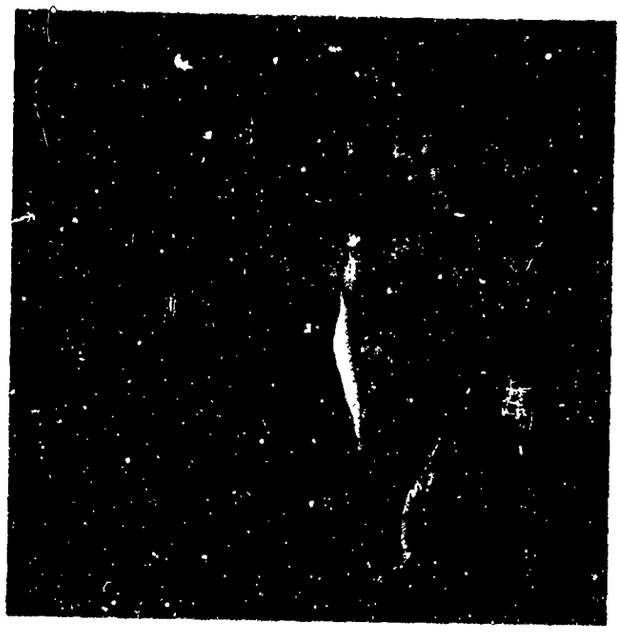

Figure 21. Transition Between Rough and Smooth Regions of $Eu_2Er_1Ga_{0.7}Fe_{4.3}O_{12}$ Epitaxial Layer. (4900X)

3.0. CHARACTERIZATION AND EVALUATION.

3.1. Chemical Analyses.

To determine the impurity content of the crystals grown in the BaO-based solvent as well as those from the PbO-based solvent, emission spectrographic analyses were performed on the crystals. To remove solvent inclusions, the samples were ground by mortar and pestle, and inclusions leached by three successive hot 20% HNO_3 extractions for periods up to three hours. Table VI shows typical impurity levels found in $YFeO_3$ samples grown from the PbO-based solvent and the BaO-based solvent. The Ba content is lower for crystals grown in BaO-based solvents, especially those grown at ~1300°C, than the Pb content of those grown by a transient method in PbO-based solvents.

The garnets which were grown from the BaO-based solvent by the transient, slow-cooled method over the temperature range of 1100-900°C were found to contain typically only 70 ppm barium.

Layers of $Eu_2ErFe_{4.3}Ga_{0.7}O_{12}$ which had grown at a temperature of 957°C onto $Gd_3Ga_5O_{12}$ substrates (but not epitaxially) were scraped off and used for emission spectrograph analysis. All of the growth solution was removed from the sample by a method similar to that developed for the orthoferrites. The amount of barium incorporated into these layers was ~24 ppm. Thus, the amount of barium incorporated in the garnets is significantly less than that found in the orthoferrites grown under comparable conditions.

TABLE VI

Typical Impurity Levels Found in $YFeO_3$ Samples Grown from PbO- and BaO-Based Solvents.

Sample from PbO-based solvent Growth Temperature 1300-900°C	Sample from BaO- based solvent Growth Temperature 1112°C	Sample from BaO-based solvent Growth Temperature 1302°C
Pb 0.1 wt.%*	Ba 0.082 wt.%	Ba 0.015 wt.%
Al 40 ppm	Al 20 ppm	Al 40 ppm
Cu < 1 ppm	Ni 40 ppm	Ni 50 ppm
Mg < 1 ppm	Si < 2 ppm	Si 3 ppm
Mn < 2 ppm	Sn 200 ppm	Sn < 4 ppm
Si < 2 ppm	Mn 4 ppm	Mn 2 ppm
Sn 30 ppm	Mg < 1 ppm	Mg 2 ppm
	Cu < 1 ppm	Cu < 1 ppm

*Values as high as 0.29 wt.% have been reported in the literature.[30]

The additional impurities in these materials stemmed from different sources. The crystalline samples were ground in an alumina mortar which may have contaminated them with aluminum. The nickel and possibly the tin in the crystals grown from the BaO-based solvent were derived from contamination of the growth solution by a piece of the apparatus, and the tin in the PbO-based solvent material was an impurity in the PbF_2 used as a solvent component.

3.2. Lattice Parameter Measurements

Since the success of heteroepitaxial crystal growth depends to a large extent upon lattice parameter match between epitaxial layer and substrate, we have measured the lattice parameters of both substrates and crystals grown in this laboratory. In some cases discrepancies exist between our data and values reported in the literature as well as between data from ceramic material contrasted to that from single crystals.

Table VII shows a comparison between between measurements on $YFeO_3$ prepared by several different techniques in this study with the best values reported in the literature. Literature values for $YAlO_3$ are also shown for comparison. Although preliminary measurements[15] indicated discrepancies between sintered polycrystalline and single crystal $YFeO_3$, the more refined measurements shown in Table VII indicate that there is very little discrepancy between samples prepared by quite different methods.

However, there has been a much more significant spread in the lattice parameters reported for $Gd_3Ga_5O_{12}$. Measurements on annealed polycrystalline material indicate that $a_o = 12.375$Å.[31] Measurements have also recently been made both in this laboratory and elsewhere on single crystals in which the lattice parameter ranges from 12.380 to 12.384Å (±0.001),

TABLE VII

Cell Dimensions of $YFeO_3$ at Room Temperature (Å)

This Study			Coppens and Eibschütz[32]	Geller[33]	$YAlO_3$[34]
Sintered Polycrystalline	Single Crystal Grown in PbO-based Solvent	Single Crystal Grown in BaO-based Solvent	Single Crystal Grown in PbO-based Solvent	Sintered Poly-crystalline	Single Crystal
a_o 5.276 ± 0.004*	5.278 ±0.003*	5.289 ±0.01*	5.2819 ±0.0002	5.280 ±0.003	5.179
b_o 5.591 ±0.002	5.590 ±0.009	5.613 ±0.008	5.5957 ±0.0005	5.592 ±0.003	5.329
c_o 7.600 ±0.002	7.604 ± 0.005	7.610 ±0.01	7.6046 ±0.0004	7.602 ±0.003	7.370

*These limits of error are derived from a least squares fit of the data and do not represent systematic errors.

depending upon the laboratory in which it is grown. There appears to be a significant variation in stoichiometry for this compound, and the lattice parameter varies with composition.[41] It is not yet clear what the optimum composition should be for lowest defect density, and in fact compositional variations have not yet been measured.

3.3. Straight Magnetic Domain Wall Apparatus.

This apparatus, described in Reference 15, was designed to permit a rapid visual examination of the quality of $YFeO_3$ crystals by revealing optically invisible defects such as internal boundaries, microscopic voids and inclusions, striations, dislocations, etc. as "hang ups" which hinder the motion of a domain wall by increasing the force necessary to move the domain wall through them. This increase in force ranges from only $\sim$1 Oe oersted for dislocations to 1000 oersteds for twin planes.[16]

The apparatus has proved very convenient for a quick qualitative evaluation and comparison of the $YFeO_3$ crystals. Slices of $YFeO_3$ prepared from both the BaO-based solvent and a PbO-based solvent have been compared, and for similar crystals (i.e., those free of obvious defects such as voids, large inclusions, grain boundaries), the crystals grown from the BaO-based solvent generally contained fewer of these invisible defects.

Figures 22a-22d illustrate the effect of increasing magnetic field upon a polished $YFeO_3$ slice containing such optically invisible defects. Several domains are present if the field is very low (Figure 22a, b). As the field is increased, only two domains remain and the domain wall between them "hangs up" at a typical defect shown in Figure 22c, then "snaps back" to its original straight line configuration in Figure 22d as the wall is passed through the crystal.

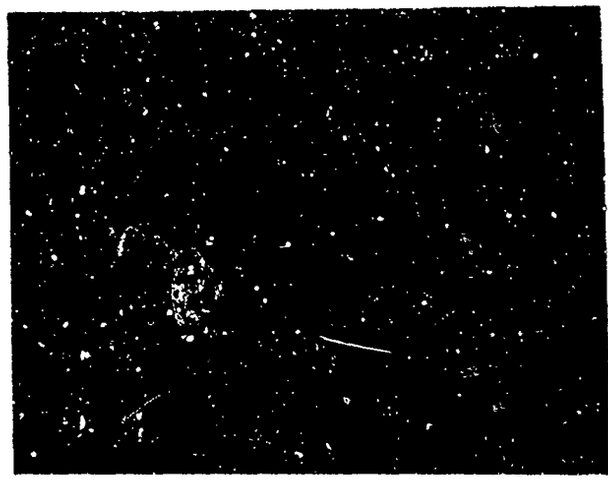

Figure 22a. Magnetic Domains in Polished Slice of $YFeO_3$ with Small Applied Magnetic Field (50X)

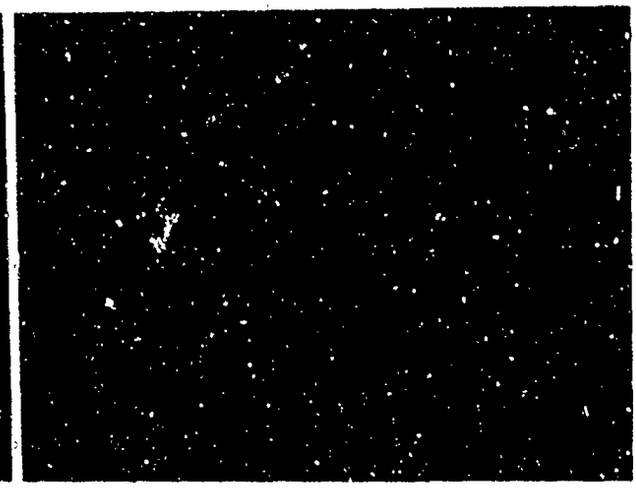

Figure 22b. Magnetic Field Increased Slightly (50X).

Figure 22c. Magnetic Field Increased Enough to Force a Straight Wall Between Two Domains in the $YFeO_3$, Except for "Hang Up" on Defect. (50X)

Figure 22d. Same Magnetic Field but Domain Wall Has Been Moved to a Defect-Free Portion of the Crystal. (50X)

3.4. Generation and Observation of Bubbles

3.4.1. Coercivity Measurements

The ultimate test of the single crystal material is the ease with which magnetic "bubbles" can be created and moved through a platelet, and experiments have been initiated to generate these bubbles and to measure the coercivity of the material and the mobility of the domain walls. Cylindrical domains are stable in a magnetic bias field of 20-90 gauss, which is provided with an external magnetic coil, and they can be generated from the serpentine domains in $YFeO_3$ and $Eu_2Er_1Ga_{.7}Fe_{4.3}O_{12}$ shown in Figures 23, 24 by means of a pulsed magnetic field caused by current pulses through a small conducting loop placed in contact with the platelet. Any strip domains passing through this loop are cut and become cylindrical under the influence of the bias field. The bubbles can be moved quite easily over the surface by applying a magnetic field gradient. An array of bubbles will align itself in a hexagonal pattern, and the coercive force can be deduced from this array (neglecting edge effects) with the aid of the relation (35)

$$\frac{H_C}{4\pi M_s} = \frac{3\pi r_o^3 h}{8\ell_{12}^4} \qquad (5)$$

where H_C = coercive force,

$4\pi M_s$ = saturation magnetization,

Figure 23a. Strip Domains in $YFeO_3$ Platelet (32X).

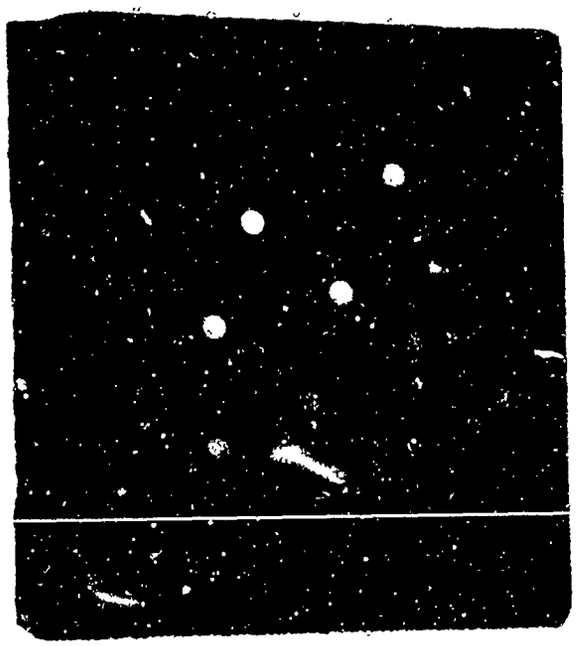

Figure 23b. Bubble Domains Generated from the Strip Domains by Increasing the Bias Field (32X).

Figure 24a. Strip Domains in $Eu_2Er_1Ga_{0.7}Fe_{4.3}O_{12}$. (400X) (Zero bias field)

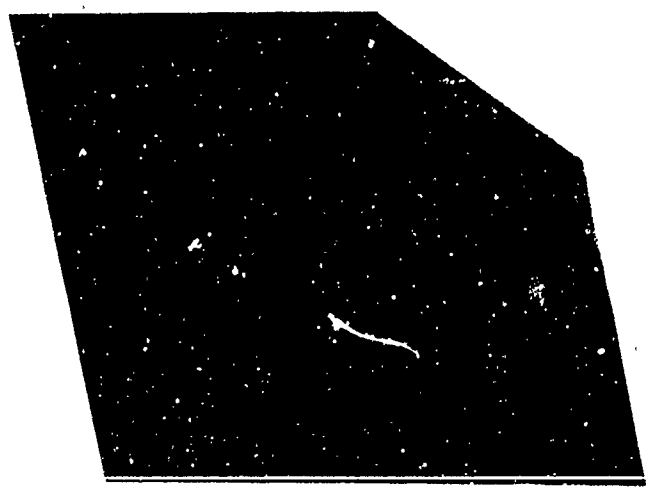

Figure 24b. Bubble Domains Generated from the Strip Domains by Increasing the Bias Field (400X). (40 oe bias field)

r_o = bubble radius,

h = thickness of the platelet, and

ℓ_{12} = distance between centers of an equilibrium array of bubbles.

The coercive force determined in this fashion for a polished $YFeO_3$ platelet grown in the BaO-based solvent has been found to be ~0.05 Oe, which is comparable to the values reported for crystals grown from the PbO-based flux after post growth annealing treatments,[36] and is well below the maximum acceptable limit of ~0.5 Oe for bubble domain devices.

3.4.2. Mobility Measurements

There are several methods currently in use to measure bubble mobility in the uniaxial magnetic rare earth compounds,[37] all of which are based upon a number of assumptions and often yield conflicting results. We have chosen the collapsing bubble technique which perhaps is the most convenient and reliable method available.

Using this technique, the measured mobilities on polished (but otherwise untreated) $YFeO_3$ platelets grown from the $BaO\text{-}B_2O_3\text{-}BaF_2$ solvents have been found to be 2000-4000 cm/sec Oe, which is again comparable to the values reported for crystals grown from the PbO-based solvents.[36]

The epitaxial layers of rare earth garnets grown to date, have been of sufficient quality to exhibit mobile bubbles, but magnetic measurements have not yet been made on them.

3.5. X-Ray Topographic Studies.

Lang and Berg-Barrett topographs have proven very useful for investigating the interaction between crystal defects and magnetic domains[37] as well as to reveal certain types of defects which are optically invisible, such as dislocations. The Berg-Barrett technique was also used for substrate surface evaluation in the epitaxial growth studies. Figures 25a,b show a portion of a $YFeO_3$ slice (flat surface perpendicular to the c-axis) as seen in optical transmission and by Lang topographic techniques. The specimen was 0.04 mm thick, and the X-ray topograph was taken with Mo radiation (50 kV, 25 mA), and was exposed for 18 hours. A number of dislocations can be seen in the left half of the crystal as well as along the upper edge. The black spots in the right lower center in Figure25b appear to be either precipitates or inclusions, or possibly dislocations, which are not visible under optical microscopy. Further studies are needed to determine the exact nature of these defects and their interaction with the domains. Portions of the crystal, such as the upper right portion in Figure 25b appear to be quite defect-free.

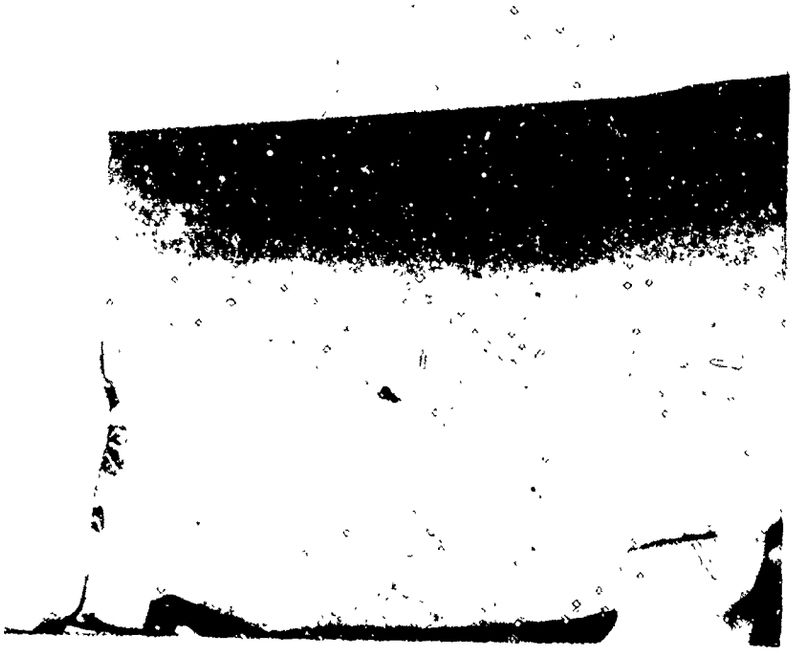

Figure 25a. Optical Transmission Photograph of $YFeO_3$ Platelet Showing Gradually Increasing Optical Absorption Toward the Top of the Platlet.

Figure 25b. Lang Topograph of Same Area as Figure 25a, Depicting Optically Invisible Dislocations (Dark Lines and Spots).

4.0. CONCLUSIONS

Controlled steady-state homoepitaxial solution growth of high quality $YFeO_3$ crystals has been demonstrated. A novel solvent, superior in several respects to conventional PbO-based solvents has been developed. This solvent, $BaO-B_2O_3-BaF_2$, is particularly advantageous when used at crystal growth temperatures in excess of 1000°C because of its very low volatility and reactivity toward the platinum crucible, even at 1300°C. $YFeO_3$ crystals grown homoepitaxially by the steady-state technique in this solvent exhibited domain wall mobilities >3500 cm/Oe-s, comparable to crystals grown in the PbO-based solvent. Barium content of these crystals was very low, ranging from 0.082 wt % in crystals grown at ~1100°C to 0.015 wt % in those grown at ~1300°C. This latter number represents almost an order of magnitude improvement over lead impurity content found in crystals grown from PbO-based solvents.

Heteroepitaxial growth of $YFeO_3$ on c-axis $YAlO_3$ substrates using the BaO-based solvent was attempted at temperatures ranging from 980-1300°C, but attack of the substrate by the solvent accompanied by formation of an intermediate layer (containing Y, Fe, Al and O) prevented epitaxy.

Magnetically uniaxial rare earth garnets, such as $Eu_2Er_1Ga_{0.7}Fe_{4.3}O_{12}$, were successfully grown heteroepitaxially on {111}

$Gd_3Ga_5O_{12}$ substrates both in the BaO-based solvent and in a PbO-based solvent. The best epitaxial layers (with respect to surface morphology and crystalline perfection) were grown at 900-300°C in the PbO-based solvent. Layers often cracked in the BaO-based solvent, apparently due to thermal expansion differences between the layer and adhering solvent during cooling. It may be possible to alleviate this problem by using modified growth techniques to minimize the amount of solvent adhering, or by adjusting solvent composition to a lower liquidus temperature.

Barium impurity contents as low as 0.0024 wt % have been found in these layers. Further investigation is needed to determine which of the two solvents is more appropriate for heteroepitaxial garnet growth in the 900-800°C temperature range.

REFERENCES

1. A. H. Bobeck, Bell Syst. Tech. J. 46, 1901 (1967).

2. P. Eisenberger, P. H. Schmidt and E. M. Walters, Appl. Phys. Lett. 17, 533 (1970).

3. S. L. Blank, L. K. Shick and J. W. Nielsen, J. Appl. Phys. 42, 1556 (1971).

4. T. Okada, K. Matsumi and H. Makino, NEC Res. and Dev. No. 19, 102 (1970).

5. L. G. Van Uitert, W. A. Bonner, W. H. Grodkiewicz, L. Pictroski, and G. J. Zydzik, Mat. Res. Bull. 5, 825 (1970).

6. L. G. Van Uitert, D. H. Smith, W. A. Bonner, W. H. Grodkiewicz and G. J. Zydzik, Mat. Res. Bull. 5, 455 (1970).

7. H. Callen, Appl. Phys. Lett. 18, 311 (1971).

8. A. Rosencwaig, W. J. Tabor, F. B. Hagedorn and L. G. Van Uitert, Phys. Rev. Lett. 26, 775 (1971).

9. A. Rosencwaig, W. J. Tabor, and R. D. Pierce Phys. Rev. Lett. 26, 779 (1971).

10. D. M. Heinz, P. J. Besser, J. M. Owens, J. E. Mee and G. R. Pulliam, J. Appl. Phys. 42, 1243 (1971).

11. E. A. Giess, B. A. Calhoun, E. Klokholm, T. R. McGuire and L. L. Rosier, Mat. Res. Bull. 6, 317 (1971).

12. L. K. Shick, J. W. Nielsen, A. H. Bobeck, A. J. Kurtzig, P. C. Michaelis and J. P. Reekstin, Appl. Phys. Lett. 18, 89 (1971).

13. L. J. Varnerin Jr., Intermag Conference, Denver, Colorado, April 1971.

14. A. H. Bobeck, E. G. Spencer, D. H. Smith and L. G. Van Uitert, Intermag Conference, Denver, Colorado, April 1971.

15. R. A. Burmeister, T. L. Felmlee and R. Hiskes, Semiannual Technical Report, Magnetic Rare Earth Compounds, Contract No. DAAH01-70-C-1106 Program Code No. OD10, December, 1970.

16. J. W. Nielsen, Metallurgical Trans. 2, 626 (1971).

17. R. C. Linares, J. Am. Ceram. Soc. 45, 307 (1962).

18. H. H. Quon and A. G. Sadler, J. Can. Ceram. Soc. 36, 33 (1967).

19. J. W. Nielsen, J. Appl. Phys. 31, 515 (1960).

20. L. Brewer, Natl. Nuclear Sci. Ser., Div. IV, 19B, p. 18.

21. D. C. Doughty and E. A. D. White, Acta Cryst. 13, 761 (1960).

22. E. A. Giess, D. C. Cronemeyer, L. L. Rosier, and J. D. Kuptsis, Mat. Res. Bull. 5, 495 (1970).

23. W. A. Tiller, J. Cryst. Growth 2, 69 (1968).

24. W. A. Tiller, to be published.

25. B. M. Wanklyn, J. Crystal Growth 5, 323 (1969).

26. L. K. Shick, J. Electrochem. Soc. 118, 179 (1971).

27. J. O'M. Bockris, J. L. White and J. D. Mackenzie, "Physico-Chemical Measurements at High Temperatures," Butterworths Scientific Publications, London, 1959.

28. D. L. Wood, J. P. Remeika and E. D. Kolb, J. Appl. Phys. 41, 5315 (1970).

29. L. K. Shick and J. W. Nielsen, J. Appl. Phys. 42, 1554 (1971).

30. J. P. Remeika and T. Y. Kometani, Mat. Res. Bull. 3, 985 (1968).

31. H. E. Swanson, M. C. Morris, R. P. Stinchfield, and E. H. Evans, "Standard X-ray Diffraction Patterns," National Bureau of Standards Monograph 25- Section 2. (1963).

32. P. Coppens and M. Eibschütz, Acta.Cryst. 19, 524 (1965).

33. S. Geller, Acta Cryst. 11, 565 (1958).

34. S. Geller and V. B. Bala, Octa. Cryst. 9, 1019 (1956).

35. A. H. Bobeck, R. F. Fischer, A. J. Perneski, J. P. Remeika and L.G. Van Uitert, IEEE Trans. on Magnetics MAG-5 544 (1969).

36. F. C. Rossol, Phys. Rev. Letters 24, 1021 (1970).

37. A. J. Kurtzig and J. R. Patel, Phys. Letters 33A, 123 (1970).

38. H. J. Levinstein and R. W. Landorf, Intermag Conference, Denver, Colorado, April 1971.

39. J. E. Mee, G. R. Pulliam, D. M. Heinz, J. M. Owens and P. J. Besser, Appl. Phys. Letters 18, 60 (1971).

40. McD. Robinson, A. H. Bobeck, and J. W. Nielsen, Intermag Conference, Denver, Colorado, April 1971.

41. T. Keig, private communication.